Climate model downscaling of Vancouver Island precipitation using a synoptic typing approach

by

Stephen Randall Sobie
B.Sc., University of Victoria, 2008

A Dissertation Submitted in Partial Fulfillment of the
Requirements for the Degree of

MASTER OF SCIENCE

in the School of Earth and Ocean Sciences

Climate model downscaling of Vancouver Island precipitation using a synoptic typing approach

by

Stephen Randall Sobie
B.Sc., University of Victoria, 2008

Supervisory Committee

Dr. Andrew J. Weaver, Supervisor
(School of Earth and Ocean Sciences)

Dr. Adam H. Monahan, Departmental Member
(School of Earth and Ocean Sciences)

Dr. John C. Fyfe, Departmental Member
(School of Earth and Ocean Sciences)

Supervisory Committee

Dr. Andrew J. Weaver, Supervisor
(School of Earth and Ocean Sciences)

Dr. Adam H. Monahan, Departmental Member
(School of Earth and Ocean Sciences)

Dr. John C. Fyfe, Departmental Member
(School of Earth and Ocean Sciences)

ABSTRACT

A statistical downscaling technique is employed to link atmospheric circulation produced by climate models at the large-scale to precipitation recorded at individual weather stations on Vancouver Island. Relationships between the different spatial scales are established with synoptic typing, coupled with non-homogeneous Markov models to simulate precipitation intensity and occurrence in historical and future periods. Types are generated through a clustering algorithm which processes daily precipitation observations recorded by Environment Canada weather stations spanning 1971 to 2000. Large-scale atmospheric circulation data is taken from an ensemble of climate model projections made under the IPCC AR4 SRES A2 scenario through the end of the 21^{st} century. Atmospheric predictors used to influence the Markov model are derived from two versions of the data: Averages of model grid cells selected by correlation maps of circulation and precipitation data; a new approach involving Common Empirical Orthogonal Functions (EOFs) calculated from model output over the Northeast Pacific Ocean. Circulation-based predictors capture the role of sea level pressure (SLP), and winds in influencing coastal precipitation over Vancouver Island.

The magnitude and spatial distribution of the projected differences are dependent on the predictors used. Projections for 2081 to 2100 made using common EOFs result in most stations reporting no statistically significant change compared to the baseline period (1971

to 2000) in both seasons. Projections using averaged grid cells find winter season (Nov-Feb) precipitation anomalies produce values that are modestly positive, with typical gains of 6.5% in average precipitation, typical increases of 7.5% rising up to 15% in extreme precipitation, and little spatial dependence. In contrast, average and extreme summer precipitation intensity (Jun-Sep) declines negligibly at most island weather stations with the exception of those on the southern and western sections, which experience reductions of up to 20% relative to the latter thirty years of the twentieth century. Precipitation occurrence decreases slightly in both seasons at all stations with declines in the total days with measurable precipitation ranging from 2% to 8% with reductions also seen in the length of extended periods of precipitation in both seasons.

Contents

List of Tables

List of Figures

ACKNOWLEDGEMENTS

I would like to thank:

Andrew Weaver, for mentoring, support, and encouragement.

the members of my committee, for guidance and advice.

my colleagues in the Climate Modelling Group for friendship and support.

my family for helping me reach this point in life.

the NSERC CREATE Training Program for providing research funding.

Einstein has somewhere remarked that he was guided towards his discoveries partly by the notion that the important laws of physics were really simple. R. H. Fowler has been heard to remark that, of two formulae the more elegant is likely to be true. Dirac very recently sought an explanation alternative to that of the spin in the electron because he felt that nature could not have arranged things in such a complicated way ...
If they would condescend to attend to meteorology the subject might be greatly enriched. But I suspect they would have to abandon the idea that the truth is really simple.
Lewis Fry Richardson

Chapter 1

Introduction

Successive reports from the Intergovernmental Panel for Climate Change (IPCC) have illustrated with increasing confidence that the added influence of anthropogenic CO_2 on the climate system will result in substantial effects on the global environment. Predictions of how specific aspects of the climate system respond to these projected changes at the scale of areas such as Vancouver Island are crucial to determining what levels of adaptation are needed over the coming decades. Among the many climatic variables whose evolution over the 20^{th} century must be known, precipitation is one of the most important due to its fundamental role in urban, rural and natural environments. Understanding future precipitation is necessary for assessing the potential risks due to factors such as flooding, forest fires and water availability. Of particular importance, a significant number of Vancouver Island communities' water supplies depend on heavily developed aquifers, which are sensitive to long-term shifts in precipitation [B.C. Ministry of Environment (2007)]. Future changes in the precipitation in regions susceptible to drought, areas of snow pack accumulation, and drinking-water reservoir basins on the island are all needed in order to prepare long-term plans for investments in precipitation related planning and infrastructure [Lemmen et al. (2007)].

Global Climate Models discussed in the IPCC Fourth Assessment Report (AR4) provide insight into how shifts in climate due to anthropogenic influence will affect coastal British Columbia (BC) [Christensen et al. (2007); Elsner et al. (2009)]. A major drawback of the

spatial resolution of climate models is the inability to resolve smaller-scale topography and local effects that create local or 'micro' climates. This is especially true for Vancouver Island, where features such as the Beaufort Mountain Range located along the length of the island, and coastal straits and fjords, are typically unrepresented. Climate model downscaling [Fowler et al. (2007); Wilby et al. (2004); Hewitson and Crane (1996)] provides a mechanism to interpret the broader, long-term projections of global climate models at the local scale. Past downscaling studies have been employed in a variety of regions such as the Hawaiian Islands [Tim and Diaz (2009)], Illinois [Vrac et al. (2007)], Scandinavia [Hellstrom et al. (2001)], or the Pacific Northwest (Northwestern United States) [Salathe (2003); Widmann et al. (2003)], among others. This project is directed solely on Vancouver Island, which possesses both the varied topography and the wide range of precipitation regimes that makes downscaling necessary to understand the effects of future climate change on precipitation.

Precipitation over Vancouver Island is defined by strong seasonal differences (Figure 1.1), with the majority of the precipitation occurring during the winter months (defined here as November, December, January and February), and with minimal precipitation during the summer months (defined here as June, July, August and September). November and September are added to the standard meteorological definitions of winter and summer, respectively because November receives the greatest total monthly precipitation and September receives the same total monthly amount as June at the majority of the weather stations on the island (Figure 1.2). The remaining months represent transition periods between the summer and winter regimes. Vancouver Island's climate is not effectively represented by the standard meteorological division of annual observations into four distinct seasons. Instead, the island's annual variations in precipitation are analogous to a form of 'Mediterranean Climate' with only two distinct seasons: wet and dry. As a result, only the extended two (extended) winter and summer seasons are needed to accurately describe the typical precipitation regimes observed on the island.

The strong shifts in precipitation intensity are driven by the seasonal changes in the direction of the prevailing winds due to variations in the strength and location of the semi-permanent air pressure cells that exist in the Northeast Pacific. In the winter months Vancouver Island typically experiences strong, southwesterly atmospheric flow as the Aleutian Low moves southward and intensifies. Advection of humid air from the subtropics towards the mid-latitudes brings more frequent and more intense precipitation events to the coast. Additionally, an increased frequency of mid-latitude cyclones reach landfall near or on the island as they are directed towards the BC coast along the northwesterly storm

tracks, driven by the polar jet stream between the Aleutian Low and the North Pacific High. During the summer months, the Aleutian Low retreats northward and the North Pacific High shifts to replace it, becoming the dominant influence on the prevailing winds. This results in weaker, northwesterly flow that transports drier air from the sub-polar regions to the mid-latitudes. The summer location of North Pacific High results in extended periods of stable, subsiding air with no significant precipitation. Precipitation that occurs is normally diverted away from the island, with moisture bearing air masses deflected to the north, towards northern British Columbia and Alaska [Mass (2008)].

While the area of Vancouver Island is relatively small, it possesses a range of precipitation regimes varying in seasonal differences and intensities, as well as a wide range of topographically distinct regions (Figure 1.3). As atmospheric flow reaches the island, orographic lifting results in enhanced precipitation on the windward sides and reduced precipitation on the leeward sides of these objects. During the winter months when the dominant atmospheric flow is from the southwest, the Beaufort Mountain Range along the length of the island generates a rain shadow across the width of the island, with greater precipitation observed on the western coast relative to the eastern coast. The flow is also interrupted by the presence of the Olympic Mountain Range to the south of the island, which significantly reduces precipitation over the southern section. In the summer months, with atmospheric flow typically originating from the northwest, the gradient in observed precipitation intensity shifts in orientation from a southwest-northeast gradient to a more west-east gradient with the greatest diminishment in precipitation experienced on the southeastern tip of the island. In both the winter and summer seasons, individual weather stations are also subject to local topographic influences resulting in variations in observed seasonal averages at stations in relatively close proximity.

As a result of these geographic and seasonal differences, the broad precipitation trends received over the island can be characterized by four representative weather stations. These have been selected as Cape Scott, Estevan Point, Victoria International Airport and Campbell River Airport. Each of these stations is located in one of four distinct precipitation regions and will be used to highlight the local-scale changes predicted by the downscaling model.

Studies involving the simulation of precipitation on the west coast have generally involved either large regions encompassing multiple provinces and states, or have employed downscaling techniques as an intermediate step between large-scale climate models and

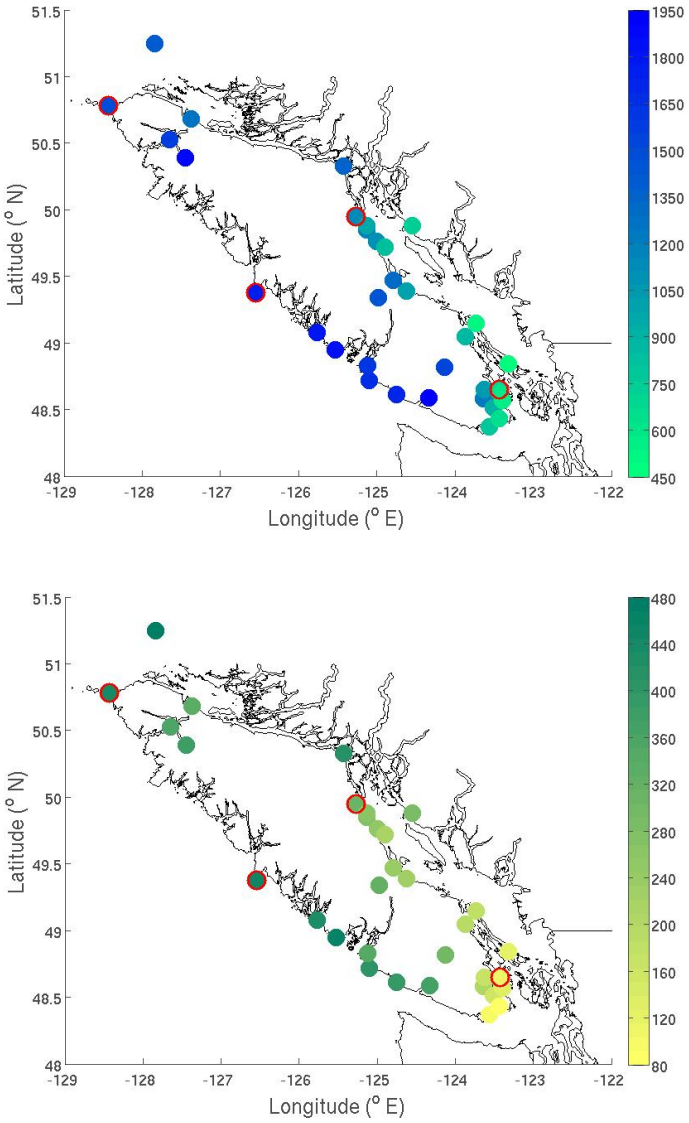

Figure 1.1: Annually averaged total precipitation (mm) over Vancouver Island spanning the years of 1971-2000 for both winter (top) and summer (bottom) seasons. The markers denote the locations of the Environment Canada weather stations used in this study, and red ringed markers identify the representative stations. Clockwise from top left: Cape Scott, Campbell River Airport, Victoria International Airport, Estevan Point.

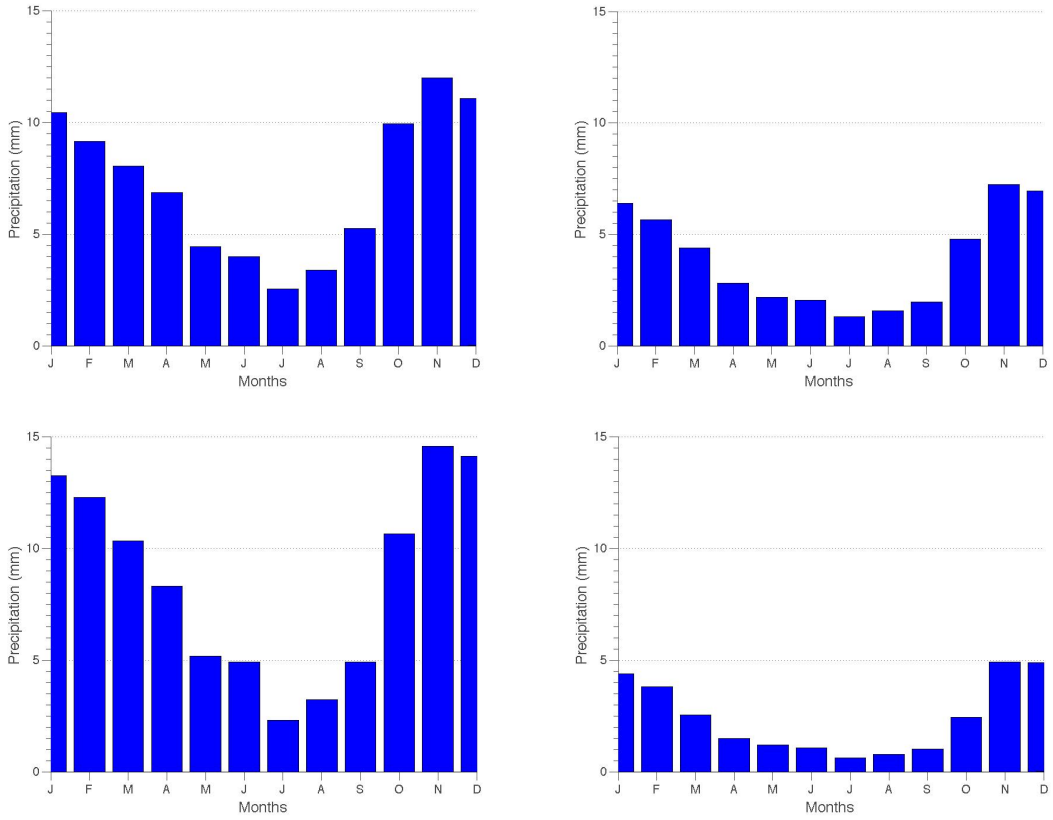

Figure 1.2: Monthly average precipitation from the four representative stations covering the four distinct precipitation regimes on the island. Clockwise from top left: Cape Scott, Campbell River Airport, Victoria International Airport, Estevan Point.

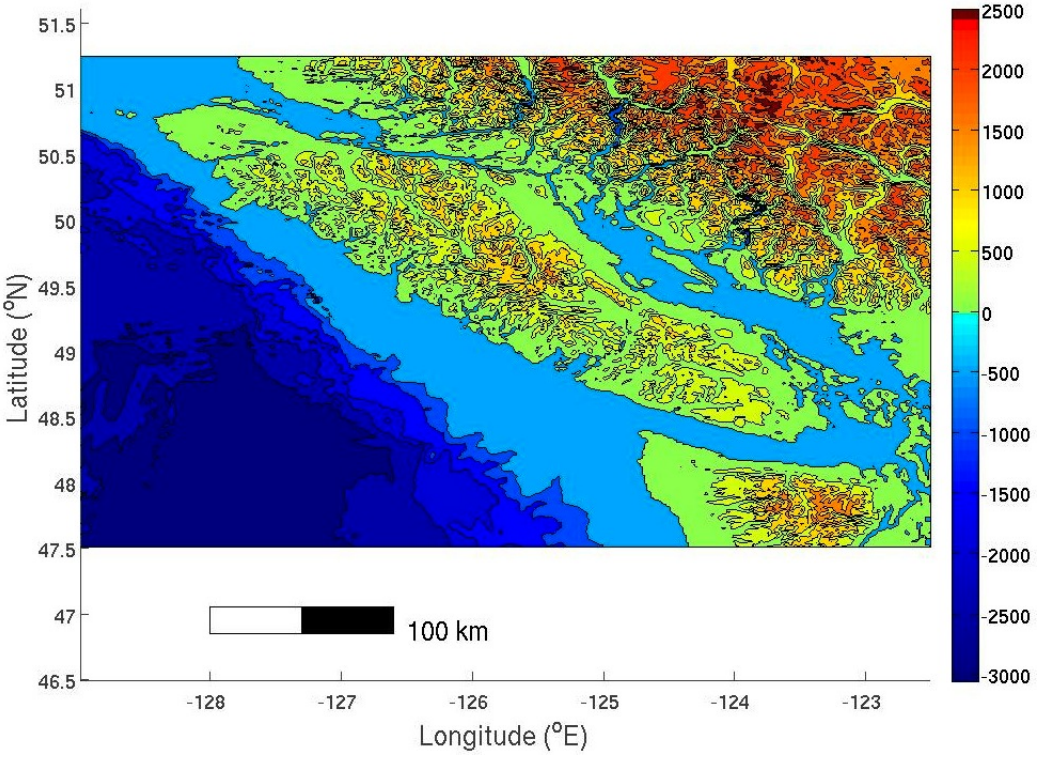

Figure 1.3: Vancouver Island with its surrounding topography of open ocean, coastal straits and mountain ranges (elevation/depth in metres).

hydrologic models [Fowler et al. (2007)]. On the Pacific Northwest and British Columbia coasts, projected increases in temperature and atmospheric water vapour result in greater precipitation intensity over the region as a whole in the winter months [Christensen et al. (2007); Held and Snoden (2006)]. In downscaling studies many previous works for the coast have regions of interest confined to the catchment basins of various river systems in the Coast and Cascade Mountain Ranges [Salathe (2005, 2003); Widmann et al. (2003)]. These studies have found that large-scale climate models have poorly replicated the reduced precipitation observed on the leeward sides of mountain ranges and other similar topographic features. Issues with a lack of observations in remote or mountainous terrain coupled with the difficulty of representing such features in the coarse resolution of most climate models has led to greater uncertainty in the projections made for those areas [Christensen et al. (2007)]. Capturing the interaction of circulation-induced precipitation and significant topography is therefore necessary as large-scale models predict increases and shifts in the magnitude and direction of the prevailing winds in the Northeast Pacific over the course of the 21^{st} Century [Merryfield et al. (2009); Milnes et al. (2010)].

The possible effect of future changes in the existing circulation patterns has been documented by previous statistical downscaling studies, which have noted distinct seasonal differences in the magnitude of precipitation projections in these mountainous regions. In the winter months when precipitation is projected to increase in intensity, differences are most acute on the windward sides of mountain ranges. There, where precipitation is most intense due to orographic lifting of incident air masses, projected increases in the prevailing winds coupled with increases in precipitable water are expected to result in enhanced precipitation [Schuenemann and Cassano (2010); Hellstrom et al. (2001)]. In contrast, while summer precipitation intensity is projected to undergo negligible change, recent downscaling results [Salathe (2005); Widmann et al. (2003)] have identified localized drying in the leeward sides of mountain ranges as the existing rain shadow is enhanced by increases in the speed of the prevailing northwesterly winds [Merryfield et al. (2009)]. These topographic effects have been a key focus of many previous hydrologic modelling studies, which often incorporate downscaling as a link between climate models and hydrologic models, in an effort to predict changes in the frequency and magnitude of flooding and drought events in mountain watersheds.

Among the many downscaling techniques available, synoptic typing methods hold key advantages for downscaling precipitation in coastal environments with significant topography [Wilby et al. (2004)]. Defining states of both atmospheric and precipitation patterns

enables the development of statistically-based relationships between the large and small scales at a variety of station environments. Each of these states represents an average of similar days of precipitation or atmospheric circulation, allowing a time series of daily data to be described by a small number of repeating patterns. For example, the sizable amount of precipitation produced by the passage of mid-latitude cyclones can be captured by a representative state associated with intense precipitation types. The changes in frequency of occurrence of these systems due to shifts in circulation patterns can then be recreated by changes in the frequency of occurrence of that synoptic type [Tim and Diaz (2009)]. The local response to long-term variability in atmospheric circulation is reflected by shifts in the frequency of occurrence of different types [Stahl et al. (2006)]. Additionally, synoptic typing of precipitation amount and occurrence using separate processes better represents the seasonal variability and persistence of precipitation events [Apipattanavis et al. (2007); Gregory et al. (1993)]. Synoptic types can be simulated in past or future periods using a variety of techniques such as logistic regression or Markov models. Homogeneous Markov models simulate transitions between synoptic states determined solely on the probabilities of occurrence seen in observations. On the other hand, non-homogeneous Markov models allow transition probabilities to be influenced by external parameters (in this case atmospheric circulation variables). This enables future transitions from synoptic state to synoptic state to include to effects of projected changes in atmospheric circulation, conditioning future projections of precipitation regimes to respond to those external influences [Vrac et al. (2007); Bellone et al. (2000); Hughes et al. (1999)].

Many previous synoptic typing approaches combine similar circulation variables into representative patterns that describe the most commonly observed circulation. They further relate precipitation patterns to the composites of atmospheric circulation [Schuenemann and Cassano (2010); Myoung and Deng (2009); Cheng et al. (2007); Vrac et al. (2007); Stahl et al. (2006); Yarnal et al. (2001); Konrad (1997)]. Increased precipitation due to shifts in atmospheric circulation patterns projected by an ensemble of climate models has been effectively captured using synoptic typing over coastal regions of Greenland [Schuenemann and Cassano (2010)]. Extreme weather events such as high intensity precipitation Konrad (1997) and freezing rain [Cheng et al. (2007)] have been linked to characteristic synoptic patterns whose magnitude and sign of response to climate change varies spatially within the study region. Using Singular Value Decomposition, Paul [Paul et al. (2008)] concluded that changes in precipitation over regions of eastern China were likely due to weakening of the synoptic scale circulation over the western Pacific Ocean. Recently however, Vrac [Vrac et al. (2007)] determined that while synoptic types derived from atmospheric circulation could effectively represent precipitation over Illinois, there was a significant improvement

in the simulation of precipitation, particularly of higher intensity events, by synoptic types developed from precipitation-based patterns.

Synoptic typing is often performed using the principal components of Empirical Orthogonal Functions (EOF) as a basis for developing the characteristic patterns of the dataset of interest. EOF analysis [Bjornsson and Venegas (1997); Wilks (1995)] has been used in the context of synoptic typing both to study the physical mechanisms for mesoscale circulation [Hannachi et al. (2007)], and to facilitate downscaling by reducing the dimensionality of large-scale datasets [Myoung and Deng (2009); Paul et al. (2008)]. Commonly, synoptic scale patterns are derived using a k-means clustering algorithm on a selected number of retained principal components [Cuell and Bonsal (2009)]. As well, predictor variables that correlate well with precipitation at a smaller scale can be derived from the principal components of the modes of variability of the EOFs [Vrac et al. (2007); Myoung and Deng (2009)].

One form of EOF decomposition that can assist in reducing the size of datasets that possess data spanning multiple time periods (such as historical and future times) is known as 'Common EOFs'. In the standard empirical orthogonal analysis, EOF decomposition is performed on the each of the time periods separately, producing separate collections of modes of variability. In this case, it is not always assured that the modes from the different times correspond with one another (e.g. EOF1 in the future is not necessarily a continuation of EOF1 from the historical period). Common EOFs are derived by taking the two datasets from separate time periods, concatenating them together, and performing standard EOF analysis on the resulting, larger dataset. As introduced by Benestad [Benestad (2001)], common EOFs provide an alternative method for the representation of the statistical modes that exist across both observed and simulated datasets. By constraining the decomposed modes of variability to span the entire range of the data from past to future eras, the modes of variability are assured to possess the same ranking in explained variance (or whatever ranking method is used) across the entire study period. This is particularly important for higher order modes, which may differ in order of explained variability when shifting from a past climate start to a future state, if the two times are evaluated separately. [Benestad et al. (2008)].

While variability in the frequency of occurrence of different synoptic states can be modelled using standard typing methods, changes in the precipitation distribution within each synoptic type are not always easily represented [Stahl et al. (2006)]. These issues are most

prevalent during shifts in long-term atmospheric variability as represented by various climate indices. Interannual variability in the frequency and intensity of the synoptic systems that supply precipitation are influenced by the yearly to decadal oscillations in the Pacific such as the El Niño-Southern Oscillation (ENSO) [Trenberth and Hurrell (1994)]. Signals from this type of variability propagate to the North Pacific through the atmospheric bridge [Alexander et al. (2002)], which links changes in the tropical Pacific Ocean to extratropical regions. This type of low-frequency variability affects changes in the strengths and positions of the semi-permanent pressure cells in the Pacific as well as the locations of the storm tracks that are responsible for bringing much of the precipitation [Stahl et al. (2006)]. Long-term shifts in the large-scale circulation fields can influence the representative synoptic types depending on which subset of the observational record is used to develop synoptic types. When days of precipitation are divided into separate precipitation types the dominant phenomenon during the typing training period (e.g. positive ENSO phase) can result in types that may be less effective at representing precipitation regimes during a different period (e.g. negative ENSO phase). This potential effect can be mitigated by specifically training and validating a typing model during different atmospheric phases, however this usually requires a lengthy dataset to capture the full range of the variability. As with all downscaling techniques attempting to predict future climates, the effectiveness of the statistical downscaling relationships can only be tested using existing data and are assumed to remain reliable into the future.

As precipitation events along the coast are linked to the patterns of atmospheric circulation over the Northeast Pacific, future projections of how these patterns are expected to differ with the effects of climate change are key to understanding potential changes in precipitation on the island. Recent studies into the future of Northeast Pacific atmospheric conditions have identified a northward shift in the both the average position of the Aleutian Low and the corresponding mid-latitude storm tracks as predicted by a range of climate models simulating the 21^{st} century [Salathe (2006); Tim and Diaz (2009); Myoung and Deng (2009); Merryfield et al. (2009)]. As the most intense precipitation associated with the storm track is situated at the southern portion of its regional extent [Salathe (2006)], any northward movement could result in greater precipitation over the Vancouver Island. The shift is analogous to the climatic changes that occur during a typical La Nina event, in which mid-latitude storm tracks move poleward and westward, and a coincident increase in precipitation occurs along the British Columbia coastline [Stahl et al. (2006); Trenberth and Hurrell (1994)]. This intensification of precipitation is evident both in the large-scale models, and in the downscaled results incorporating those large-scale processes [Salathe (2006)].

The present study aims to determine how precipitation over Vancouver Island is projected to evolve through to the end of the 21^{st} century under the influence of climate change. It will measure the ability of a downscaling technique based on the synoptic typing of observed precipitation to replicate current precipitation records and to predict future precipitation trends using modelled atmospheric circulation patterns. The downscaling model will be used in a region not yet subjected to statistical downscaling involving precipitation, and will be the first time that this method is employed in a coastal environment. The following section presents the methodology employed in the study, describing the global climate model evaluation, large-scale predictor selection, and validation and projection techniques. In the third section, the results of the model training, validation and projection are described, focusing on the individual station results using the different predictor selections. Finally, a summary of the downscaling model's effectiveness is presented with comments on the model's uncertainties and shortcomings.

Chapter 2

Methodology

2.1 Data

Climate data used for downscaling in this study consisted of precipitation observations, reanalysis products, and global climate model output from a range of models. Observations of precipitation were obtained from the Environment Canada Weather Office Climate Data Online service at *http*: *//www.climate.weatheroffice.gc.ca/climateData/canada_e.html* [Environment Canada (2010)]. These data were recorded by weather stations in both urban centres and remote locations, such as lighthouses, located mainly around the periphery of Vancouver Island. The time series of daily precipitation totals from 1971-2000 were taken from weather stations with continuous records missing fewer than five percent of the total number of days in the record. Thirty-four weather stations satisfied these criteria, and the observations from these weather stations were used to derive downscaling relationships to the large-scale climate model output.

Large-scale climate variables during the 20^{th} century were obtained using the National Centers for Environmental Prediction (NCEP) Reanalysis Products [Kalnay and coauthurs (1996)]. NCEP data was provided by the NOAA/OAR/ESRL PSD, Boulder, Colorado, USA, from their Web site at *http*: *//www.esrl.noaa.gov/psd*. Atmospheric circulation variables from 1971-2000 over the Northeast Pacific (spanning the coordinates 10^oN to 75^oN

and -200^oE to -100^oE) were acquired from the reanalysis dataset. NCEP Reanalysis variables are generated through a combination of observations and output from a numerical weather prediction model. The same numerical model is used to produce short term predictions of meteorological variables which are then compared to observations during the same period. The observations are then used to corroborate or correct the model simulations and the reanalysis data is produced from the assimilation of these two components. In regions where observations are sparse, the reanalysis data is composed primarily from the numerical model output. This is also true for meteorological variables that were not recorded by observations, or are not easily derived from observations. While NCEP Reanalysis variables are based on both weather forecasting model and observational data, they are hereafter referred to as historical climate data and will be used as a standard to identify circulation patterns and to compare climate model performance.

Global Climate Model data were retrieved from the Earth System Grid CMIP3 Multi-Model Data Portal $https://esg.llnl.gov:8443/home/publicHomePage.do$ [Meehl et al. (2007)]. All of the model simulations examined were produced for the IPCC Fourth Assessment Report [Christensen et al. (2007)]. The climate models used in this study were selected with regard to the following guidelines: they possessed daily output for a wide range of climatic and atmospheric circulation variables; the climate model conducted experiments with both the 20^{th} Century climate and SRES A2 Scenarios [Nakicenovic and coauthors (2000)]. The A2 Scenario was chosen to explore projected climate change impacts on precipitation under a more significant emissions pathway. Models that satisfied these criteria were then subjected to a series of statistical measures comparing their performance (described below) to the reanalysis record to determine if any model was significantly inferior relative to the others and required removal from the study. The models that were retained for use in this study are the Canadian Centre for the Climate Modelling and Analysis (CCCMA), le Centre National de Recherche Météorologique (CNRM), the European Centre Hamburg Model (ECHAM), and the Geophysical Fluid Dynamics Laboratory (GFDL) organizations. As each climate model was provided at a different spatial resolution, all of the models were regridded using a cubic spline interpolation scheme to the same scale as that of the NCEP reanalysis data (2.5^o square grid cells).

2.2 Methods

2.2.1 Climate Model Selection

To gauge the ability of each of the selected global climate models to replicate the historical atmospheric circulation patterns, model output was compared to NCEP Reanalysis data using three statistical metrics: Mean Absolute Error (MAE), EOF Skill Score (ESS), and Mean Logarithmic Variance (MLV) [Tim and Diaz (2009)]. MAE evaluated the climatology generated by the models against the observed climatology from the reanalysis data. ESS compared the first ten modes of variability obtained using Empirical Orthogonal Function (EOF) analysis to determine how well the spatial variability is replicated. ESS ranges in value from zero to one, with one being a perfect match between the model and reanalysis modes of variability. MLV measured the degree to which the model and reanalysis data differ in variance. An MLV value of one defines a difference of one order of magnitude between the model variance and the reanalysis variance. Each of the measures compared different aspects of the circulation represented by the atmospheric variables of sea level pressure, meridional winds and zonal winds. Data from both the models and the reanalysis data were compared separately for the summer and winter seasons over the entire Northeast Pacific domain of interest for this study. The relative performance of the models was compared and any model that was consistently poorer in replicating the NCEP fields was dropped from consideration.

2.2.2 Predictor Selection

In the development of statistical downscaling relationships, the selection of the best large-scale predictor variables that are most closely linked to the small-scale observed precipitation is essential for generating accurate small-scale projections. The selection of those atmospheric circulation variables that strongly influence local precipitation was done by considering both the regional climate dynamics (which variables are most important in defining the typical circulation), and by constructing heterogeneous correlation maps between the NCEP Reanalysis data and the weather station data (heterogeneous correlation maps compare variables at different spatial scales). Several circulation-related variables (e.g. MSLP, winds, vorticity) at several geopotential heights were compared to the observed pre-

cipitation over the historical period. The predictors were selected from model grid cells spanning the coordinates 75^oN to 10^oN and -200^oE to -100^oE. This region encompassed the western and southern extents of the mid-latitude cyclone storm tracks that transport significant amounts of moisture to the west coast of North America, as well as the areas of influence of the semi-permanent pressure cells. Domains for each predictor were identified from within this region by correlation maps. These were used to constrain the areas where the potential predictors showed the strongest relationships to the observed precipitation.

Predictor variables were extracted from the large-scale climate model output in two ways: first, the spatial average of each selected variable over an area defined by the correlation maps as being influential in determining precipitation was taken; second, a selection of principal components of each of the predictors' EOFs from the common EOF analysis were used. Both predictor selections were an attempt to employ predictor variables that represented the connection between variability at the large-scale and observations at the small-scale while reducing the size of the datasets. In the case of the spatially averaged grid cells, the correlation maps reduced the areal extent of the predictor data to regions in relatively close proximity to Vancouver Island. In the interest of examining whether other regions of the study were important in influencing precipitation, the predictors obtained with principal component analysis were taken from the entire Northeast Pacific region. However, because only a limited number of the modes of variability from certain circulation variables were used as predictors in the case of the common EOFs, some of the high-frequency components were not included as factors in driving the statistical model. The inclusion of the spatially averaged grid cells helped to ensure that all temporal components of the atmospheric signal were retained and thus could potentially influence simulation of future precipitation.

The selection of the particular atmospheric circulation variables that were relevant to influencing Vancouver Island precipitation was performed using a combination of correlation maps and a stepwise selection technique. Correlation maps provided a measure of the relationship between the individual reanalysis grid cells from the large-scale and the observed precipitation time series from the island weather stations. The choice of which predictors to include in the downscaling model was determined using a stepwise selection technique similar to those used in multivariate regression [Wilks (1995)]. In this method, each of the potential predictors was tested individually with the downscaling model applying a cross-validated approach during the historical baseline (described below). The predictor that resulted in the best agreement between the simulated values and the observations was then

retained. Successive predictors were found in the same way, with each candidate tested with the set already chosen and the most successful addition was again kept as a predictor for the statistical model. The order in which individual predictors were added was determined solely by the choosing the predictor that most improved the performance of the downscaling model. The ability of each potential predictor variable to recreate the observed precipitation statistics at all of the weather stations was measured using the statistical metric of mean squared error (MSE). Predictor variables were successively selected until the MSE was observed not to improve further with the addition of other predictors.

While the stepwise selection technique provided an objective method to determine which predictors should be employed for the downscaling model, because of the large number of potential predictors for the method to select, there was potential for overfitting when the downscaling model was tested. Overfitting could occur if multiple predictors shared similar variance structures in their time series, or had significant correlation with one another (a concept known as collinearity). At the 5% significance level, this implied 1 in 20 predictors could result in an improvement of the fit of the model solely by random processes. If the downscaling model selected these similar predictors, it would likely fit the observations more effectively, but could reduce the model's ability to predict future values. Employing a cross-validated approach to verify the ability of the downscaling model helped to reduce the possible effects of overfitting as it tested the model's ability to reproduce a subset of the data not used to train the model. However, due to the number of predictors tested and the fact that atmospheric variables such as sea level pressure and winds were not likely to be completely statistically independent, there remained the possibility of fitting the observations too well at the expense of the predictive skill of the model.

If during the course of predictor selection no moisture related variables were selected, the specific humidity at 500 hPa height was added automatically (500 hPa height chosen based on the results of the correlation maps). Specific humidity accounts for the importance of changes in water vapour to the atmospheric component of the hydrologic cycle. Although this term's importance may be small with regards to typical precipitation conditions, it is expected to undergo significant change in the course of projected climate change [Schuenemann and Cassano (2010); Hellstrom et al. (2001)]. Specific humidity influences precipitation as it is a measure of the amount of precipitable water in the atmosphere. Due to its nonlinear relationship with precipitation, specific humidity is not always selected as a predictor variable. However, its key role in the hydrologic cycle makes including it in the suite of predictors important. Past downscaling studies have noted improvement

in the performance of other downscaling methods, and it has become common to ensure some measure of atmospheric moisture content is included when attempting to downscale precipitation.

2.2.3 Downscaling Model Validation

The downscaling technique's effectiveness at recreating observed precipitation was validated by comparing the statistics of the seasonal periods under consideration, obtained both from observations and simulations. While the downscaling method offered daily precipitation values in the same format as the daily observations of precipitation totals, direct day to day comparisons between simulated and observed data were not feasible due to the stochastic nature of the downscaling process. In the case where model data was used there was no guarantee that the modelled atmospheric data was in phase with the NCEP circulation data, meaning the simulated precipitation values were not likely to coincide with the observations. Because of this, comparisons between downscaled precipitation and observed precipitation were only done in the context of the average and extreme precipitation values at each individual station in a specified season, averaged over the number of years in the simulation period in question.

Validation of the different statistical downscaling methods was performed using two separate approaches to partition the observational record. The first approach involved dividing the thirty-year observational dataset in half (two fifteen-year segments). The downscaling methods were fit or "trained" using one half of the data and then used to recreate the observations obtained during the other half of the record (split-record). This method ensured the validation component was completely distinct from the training component when calculating the overall bias of the downscaling model. The second approach, cross-validation, involved repeated asymmetrical divisions of the dataset to obtain several values of fit that could then be averaged. In the case of the thirty-year dataset, twenty-five years of data were used to construct the downscaling functions while five years of observations were set aside for validation. This division of data was repeated (six times in this case) until all years in the dataset had served as part of the validation set. This approach gives a fully cross-validated prediction - each 5 years of prediction are obtained from a model using 25 other years of data. The correlation between prediction and observation can then be made over the full record.

2.2.4 Statistical Downscaling Method

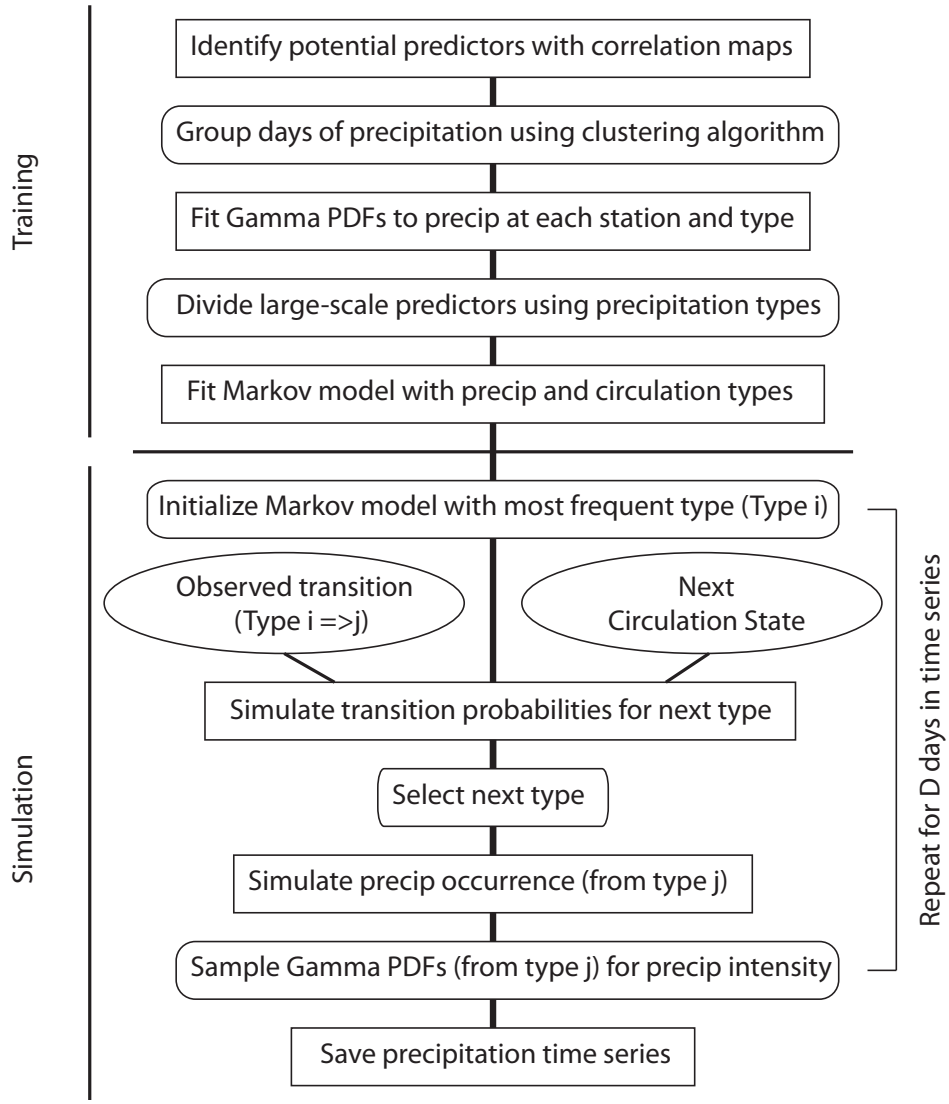

Figure 2.1: Flowchart depicting the downscaling model. The schematic is applied for each season, at each weather station, in validation and projection experiments.

The primary method of downscaling precipitation employed a statistical modelling technique derived from Vrac [Vrac et al. (2007)] to predict daily precipitation based on synoptic typing with a Nonhomogeneous Markov Model [Charles et al. (2004); Bellone et al. (2000); Hughes et al. (1999)]. In this method, synoptic types for Vancouver Island were obtained using cluster analysis of rainfall distribution at weather stations across the island. Each synoptic state was associated with a particular probability, pattern and intensity of precipitation over all weather stations. The method fit unique Gamma Probability Distribution

Functions [Bridges and Haan (1972)] to precipitation observations (r) in each synoptic type at each station creating a record of the typical precipitation associated with particular atmospheric conditions (2.1).

$$f(r|\alpha,\beta) = \frac{\beta^{\alpha}}{\Gamma(\alpha)} r^{\alpha-1} exp(-r\beta) \tag{2.1}$$

The form of the Gamma PDF is defined by two parameters: α, the shape parameter that determines whether the curve is exponential or extreme-valued in appearance; β, scale parameter, which controls the spread of the curve. The PDF also employs $\Gamma(\alpha)$, the standard gamma function.

Development of synoptic types was performed using an hierarchical ascending clustering algorithm, which compared days of precipitation distribution. The algorithm compared the similarity of different days by evaluating a distance measure that determined the relative differences in magnitude and distribution of precipitation among the weather stations. States of precipitation were defined using an original distance measure devised by Vrac [Vrac et al. (2007)]. This original metric was required to handle days with precipitation amounts close to zero and to separate the days into types based on their mean precipitation amounts rather than their maximums, as would be the case with the standard Euclidean distance metric.

Coupled with the information regarding precipitation, each synoptic type was associated with a characteristic pattern of circulation in the atmosphere, which was determined by the averaging of the atmospheric conditions during the groups of days divided according to synoptic type. The individual discretized states were not meant to explicitly determine the physical processes governing each different precipitation regime, rather they were necessary divisions of the historical data to use in this particular downscaling model. The information obtained from these constructed states was then used to simulate precipitation for validation or future periods.

The metric was evaluated for all possible pairings of different days t and t' in the observed dataset. It compared the distance measures between each of the N stations and grouped together the pairings that were the lowest. The metric not only examined precipitation intensity R_{ti}, but also their spatial and temporal distributions given by Sa_{ti} and Ta_{ti}. This

enabled the metric to discern patterns amongst the precipitation records, causing it to group together days that were similar in precipitation spatial distribution as well as magnitude.

$$Sa_{ti} = R_{ti} - \frac{1}{N}\sum_{i=1}^{N} R_{ti} \tag{2.2}$$

$$Ta_{ti} = R_{ti} - \frac{1}{T}\sum_{t=1}^{T} R_{ti} \tag{2.3}$$

The algorithm was initialized by setting each individual day as a group, and then joined together the pair of days that formed a single group with the smallest intragroup distance as defined by the distance metric defined below. The algorithm then joined the next two groups that would again minimize the intragroup distance and repeated this process until only a small number of groups, or synoptic types, had been identified. The precise number of groups that would remain at the end of this process was determined by analyzing the growth in intragroup distance as successive groups were combined [Wilks (1995)]. The cutoff point for selecting the final number of clusters was determined by stopping the algorithm when the intragroup distances reached 10% of the total possible intragroup distance (the distance if all days belonged to a single group) [Stahl et al. (2006)]. The selected cutoff point was found to form reliably a similar number of clusters (4-7) using different subsets of the historical data, and was chosen due to the rapid increase in intragroup distance that occurred if clusters were continued to be grouped after this point.

The original metric for precipitation ($d(P_{ti}, P_{t'i})$) was composed of the Bivariate Euclidean Distance (E_d) calculation between the spatial and temporal distributions as well as terms to account for amounts of precipitation $h(R_{ti}, R_{t'i})$, and a penalty term for no precipitation at all (α). For brevity, the precipitation characteristics R_{ti}, Sa_{ti} and Ta_{ti} are referred to collectively as P_{ti}.

$$d(P_{ti}, P_{t'i}) = E_d[(Sa_{ti}, Ta_{ti}), (Sa_{t'i}, Ta_{t'i})] + h(R_{ti}, R_{t'i}) + \rho \tag{2.4}$$

$$E_d[(Sa_{ti}, Ta_{ti}), (Sa_{t'i}, Ta_{t'i})] = \sqrt{((Sa_{t'i} - Sa_{ti})^2 + (Ta_{t'i} - Ta_{ti})^2)} \tag{2.5}$$

The metric was calculated at the i^{th} station for each possible day-to-day pair in the dataset. If a pair of days recorded zero precipitation ($R_{ti} = 0$ and $R_{t'i} = 0$), then the original metric $d(P_{ti}, P_{t'i})$ was assigned a value of 0. Otherwise its value was determined from equation 2.4 above.

The additional terms in the distance metric accounted for differences between precipitation intensity and when one of the two days compared recorded no precipitation at all. $h(R_{ti}, R_{t'i})$ compared the absolute difference between precipitation amount. ϵ and ρ were both empirically derived constants from the original study, defined as 10^{-3} and 1, respectively. These parameters were only included if one of R_{ti} or $R_{t'i}$ was zero.

$$h(R_{ti}, R_{t'i}) = |log(R_{ti} + \epsilon 1_{R_{ti}=0}) - log(R_{t'i} + \epsilon 1_{R_{t'i}=0})| \tag{2.6}$$

$$\rho = \frac{1 \; if \; R_{ti} or R_{t'i} = 0}{0 \; otherwise} \tag{2.7}$$

For each possible day-to-day pairing, the sum of the distance metrics at all of the N stations ($D(P_t, P_{t'})$) was evaluated. This information was then used to determine the composition of the different synoptic types.

$$D(P_t, P_{t'}) = \sum_{i=1}^{N} d(P_{t,i}, P_{t',i}) \tag{2.8}$$

A hierarchical ascending clustering algorithm using the Ward criterion W (or Wards minimum variance method) was applied to group the different days into clusters of similar types. Ward's criterion [Wilks (1995)] selected which two days or groups to cluster together

based on which of the possible pairings minimized the information loss. This was defined as the sum of squared distances between the n_g constituents of each of the G groups and their respective centroids, defined as $\bar{D_g}$ (Here n_g referred to the number of days that were grouped together in a particular group G). Clustering was performed until the number of remaining groups had decreased to a point after which reducing the groups (from G to $G-1$) would have increased the intra-group distances (or information loss) to an unacceptably high level as mentioned previously.

$$W = \sum_{g=1}^{G} \sum_{n=1}^{n_g} (D_n - \bar{D_g}) \tag{2.9}$$

Once the synoptic types were established, the observed precipitation grouped within each type at each station was fitted with a gamma distribution, and analyzed to determine the probability of precipitation.

To simulate daily precipitation values, the frequency of occurrence of the synoptic types during the training period was recorded in the form of a matrix of transition probabilities from one state to the next (γ_{ij}), and used to help determine predicted precipitation. While the probability of being in a given type based solely on the nature of the previous type would remain fixed for the entirety of the simulation, the inclusion of atmospheric variables in calculating the probability of transition enabled selection tendencies to change with evolving atmospheric conditions. The selected circulation variables were represented by a normally distributed term including the homogeneous Markov model, where X_t was the matrix containing the predictor times series of each of the circulation variables, μ_{ij} was the mean vector of the atmospheric variables when the previous synoptic type was i and the current type is j, and Σ was the covariance matrix of the atmospheric variables. γ_{ij} represented the homogeneous component of the Markov model and incorporated the transition probabilities from the observed state transitions, from type i to type j. These were obtained by examining the observed transitions that occurred during the historical period.

$$P(S_t = j | S_{t-1} = i, X_t) \; \alpha \; \gamma_{ij} \; exp[\frac{-1}{2}(X_t - \mu_{ij})\Sigma^{-1}(X_t - \mu_{ij})^T] \tag{2.10}$$

After incorporating the atmospheric components, the transition probabilities for going from state i to state j were renormalized to sum to one again. A multivariate normal distribution was chosen to represent the atmospheric variables as each of the predictors possessed differently distributed characteristics (positive or negative skewness, for example) and the normal provided a distribution that was best able to describe the combination of these different variables simultaneously [Hughes et al. (1999)]. Establishing the distribution for $P(S_t = j|S_{t-1} = i, X_t)$ required fitting a significant number a parameters to the observational dataset.

For a model with five predictor variables and five synoptic states, the downscaling model requires fitting 165 parameters to a dataset of 5400 or 9000 data points depending on whether the split-record or cross-validation approach is used. The 165 parameters are required to fit the γ_{ij} (25 parameters), μ_{ij} (125 parameters), and Σ (15 parameters) terms in the above equation (assuming 5 predictors, 5 states). These parameters are fit from the seasonal (4 months, 120 days) datasets of the 5 predictor variables and precipitation state transitions, amounting to 21600 data points over the 30 years of the observational period. Fitting the model reduces under the split-record approach reduces this to 10800 data points as 15 years are used to train the model. A further assumption of a two-day autocorrelation in the data due to the persistence of precipitation states results in a decrease in the number of independent data points by half again to 5400 data points. A similar process yields 9000 data points for the cross-validation approach. Fitting this many parameters to a finite dataset can decrease the resolution of the fitted parameters, that is their exact value may not be as precisely determined as would be the case for fewer unknowns and a larger dataset. This may introduce a further element of uncertainty in the simulated values of precipitation produced by the downscaling model.

The Markov model with the atmospheric component was also applied to the probability of precipitation occurrence calculations, where the prevalence of days with nonzero precipitation could change as well under changing circulation. For each observed day in the different synoptic types, the record of whether or not precipitation occurred was accumulated to determine the frequency of days without precipitation at each weather station. These values, along with the circulation variables, were fitted using a separate Markov model to develop a predictive equation for the probability of precipitation in the future specific to each site. Here, the same atmospheric components X_t were used as well as a distinct homogeneous Markov model that was obtained in a similar fashion to precipitation amount as described above [Apipattanavis et al. (2007); Gregory et al. (1993)].

Simulation of future precipitation for a particular day was performed by a series of steps: first, the synoptic state was determined using a Nonhomogeneous Markov model; second, prediction of precipitation occurrence based on the probability of precipitation Markov model; third, if precipitation was projected to occur, simulating the magnitude by randomly sampling the Gamma PDF for that station and state. Multiple iterations of this algorithm were performed for the different dataset divisions and predictor types.

The statistical model was validated using both the split-record and cross-validation approaches using the predictors from the averaged set of grid cells selected from the variables identified the correlation maps, and the principal components of the variables spanning the Northeast Pacific Ocean. Data used for the validation simulations were obtained both from the NCEP Reanalysis and from the ensemble of climate models. In the case of climate model data, two methods of averaging the different model simulations were applied. First, the statistical model was used with one model at a time, and the results were combined together afterwards in an unweighted ensemble. Second, the climate model projections were concatenated together to produce a single, large dataset four times as long was the case for one model for simulation purposes (described here as the "common cluster" approach). Because of the stochastic nature of the simulation process in all of the projection versions, from the simulation of synoptic type to the sampled amount of precipitation, the statistical model was repeatedly evaluated for the validation and projection periods.

Chapter 3

Results

3.1 Climate Model Output

As the downscaling model employed in this study relies on atmospheric circulation to influence simulated precipitation, the ability of different climate models to recreate the observed dynamics must be evaluated. To determine which of the four climate models identified as possessing the necessary circulation data are best suited for use in this study, a series of metrics are used to compare model data (sea level pressure, meridional and zonal winds at 850 hPa) to NCEP reanalysis data. Results of applying the MAE to both summer and winter seasons reveal that no one model is superior or deficient relative to the others, and that there is not any seasonal difference in the models' performances (Figure 3.1) in terms of Mean Absolute Error values of the selected circulation variables. MAE values range from 1.3 hPa in the winter for the CCCMA model, to 4.4 hPa in the summer for the CNRM model. Wind values are mostly clustered around 1.0 m/s in both the zonal and meridional cases, except for an outlier of GFDL zonal wind at 5.4 m/s. Comparing the other measures of ESS and MLV finds similar results in that no particular model or season shows demonstrably good or poor performance next to the others. Mean sea level pressure appears to be the most successfully recreated variable in all of the models, replicating both the variability identified by the EOF modes and in the magnitude of the variance. Meridional and zonal winds are both produced less effectively than sea level pressure by the models, with both

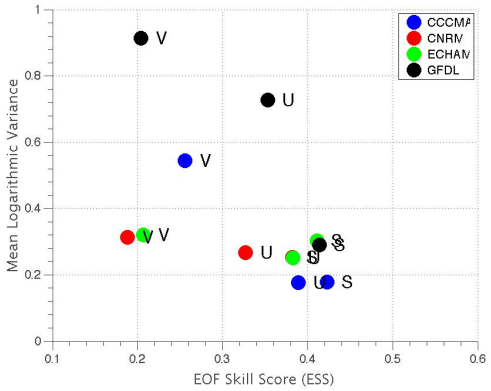

(a) Winter MLV and ESS Metrics

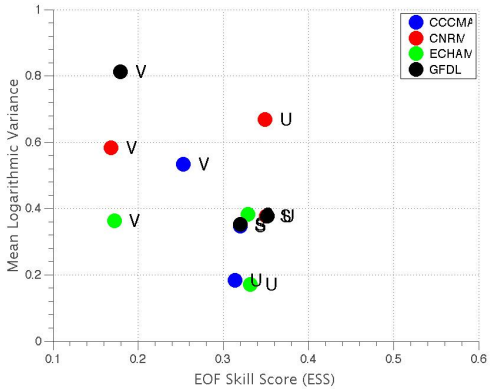

(b) Summer MLV and ESS Metrics

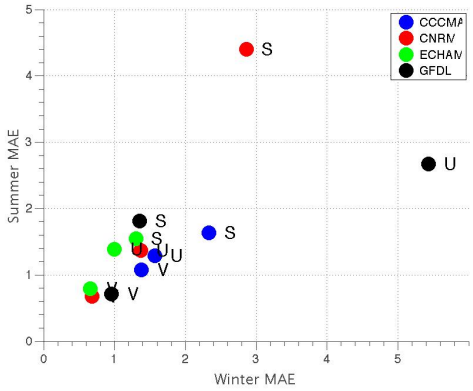

(c) MAE Winter and Summer Metrics

Figure 3.1: Evaluation of the four selected climate models performance relative to NCEP Reanalysis using three statistical metrics over the time interval of 1971-2000. S represents mean sea level pressure, U represents zonal wind speeds at 850 hPa, and V represents meridional wind speeds at 850 hPa. In both the Mean Absolute Error and Mean Logarithmic Variance metrics, a smaller value indicates better agreement with the reanalysis data. An ESS value of one describes a perfect match between the EOF modes in the model and the reanalysis modes. No single model can be eliminated from consideration using these results.

poorer ESS and MLV values in summer and winter. However, these results are common to all of the different models' output and thus one specific model cannot be eliminated as a result.

To understand the climate models interpretation of how circulation pattern changes over the 21^{st} century are reflected in the precipitation totals, the large-scale, seasonally-averaged precipitation at a representative grid cell over Vancouver Island (located over the Northwestern tip) is examined from the ensemble of the four selected models (Figure 3.2). During the winter months the projected precipitation shows a significant, increasing trend from beginning to end of the 21st century in both the average and extreme precipitation. Monthly average precipitation rises from 7.6 mm/day during the 20^{th} century to a value of 8.8 mm/day by the end of the 21^{st} century, amounting to an increase of 16%. Extreme precipitation follows a similar pattern, with an increase of 19% from 24.5 mm/day in the 20^{th} century baseline period to 29.1 mm/day in the future projection period. In the summer months, average precipitation decreases from 3.7 mm/day during the 20^{th} century to 3.4 mm/day by the end of the 21^{st} century, a decline of 8%. In contrast, extreme precipitation grows slightly, with an increase from 13.8 mm/day to 13.9 mm/day amounting to a 0.7% growth over the 100 years. While these projections describe changes at a single grid cell positioned over the northern tip of Vancouver Island, the trends at other grid cells encompassing other areas of the island show similar trends as well, if only slightly different in the magnitude of their projected change.

Individual predictor variables are determined using a stepwise selection technique in which the relative importance of each predictor in affecting precipitation is evaluated. Following the selection process described in more detail in the methodology, the predictors chosen to downscale precipitation were: Zonal Wind at 700 hPa, Mean Sea Level Pressure, Meridional Wind at 1000 hPa, Geopotential Height at 850 hPa. Additionally, specific humidity at 500 hPa was also included to account for the strong influence of changing atmospheric moisture on projected precipitation. The domains of each selected predictor can be associated with significant physical mechanisms that are strongly linked to precipitation on Vancouver Island as identified by the correlation maps (Figure 3.3). The areas of SLP and geopotential height identified by the selection process are constrained to the Northeast Pacific, specifically the Gulf of Alaska. The meridional and zonal wind fields are most strongly correlated with precipitation in the areas directly over, and to the southwest of Vancouver Island. These illustrate the influence of the westerly winds in transporting maritime air masses from the subtropical Pacific Ocean to Vancouver Island.

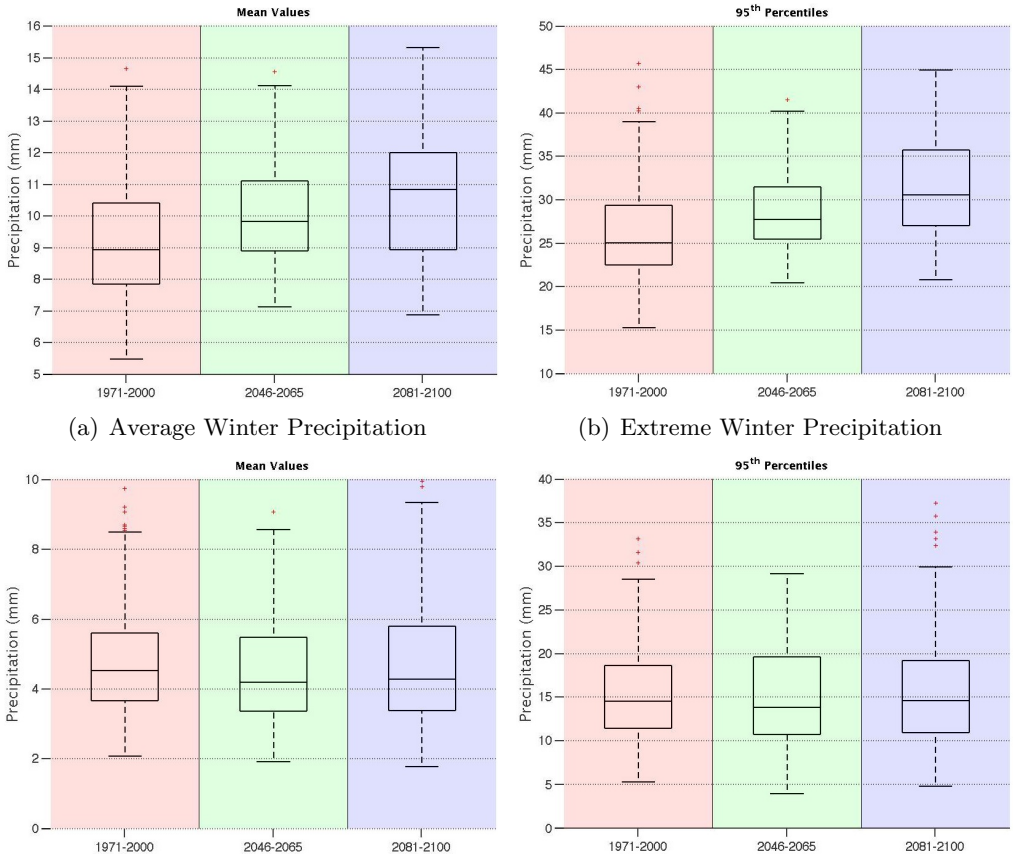

(a) Average Winter Precipitation

(b) Extreme Winter Precipitation

(c) Average Summer Precipitation

(d) Extreme Summer Precipitation

Figure 3.2: Box plots of the Multi-model ensemble predictions of the evolution of Vancouver Island seasonally averaged, daily precipitation over the 21st century during the winter and summer seasons. The precipitation data is taken from large-scale, climate model output grid from a grid cell positioned over the northwestern corner of the island. The central line in the middle of the box is the median value, the box edges are the 25^{th} and 75^{th} percentiles, and the outer whiskers are the 1^{st} and 99^{th} percentiles. Red crosses are considered outliers. Projected winter precipitation intensity displays a statistically significant, increasing trend, while summer precipitation intensity remains constant.

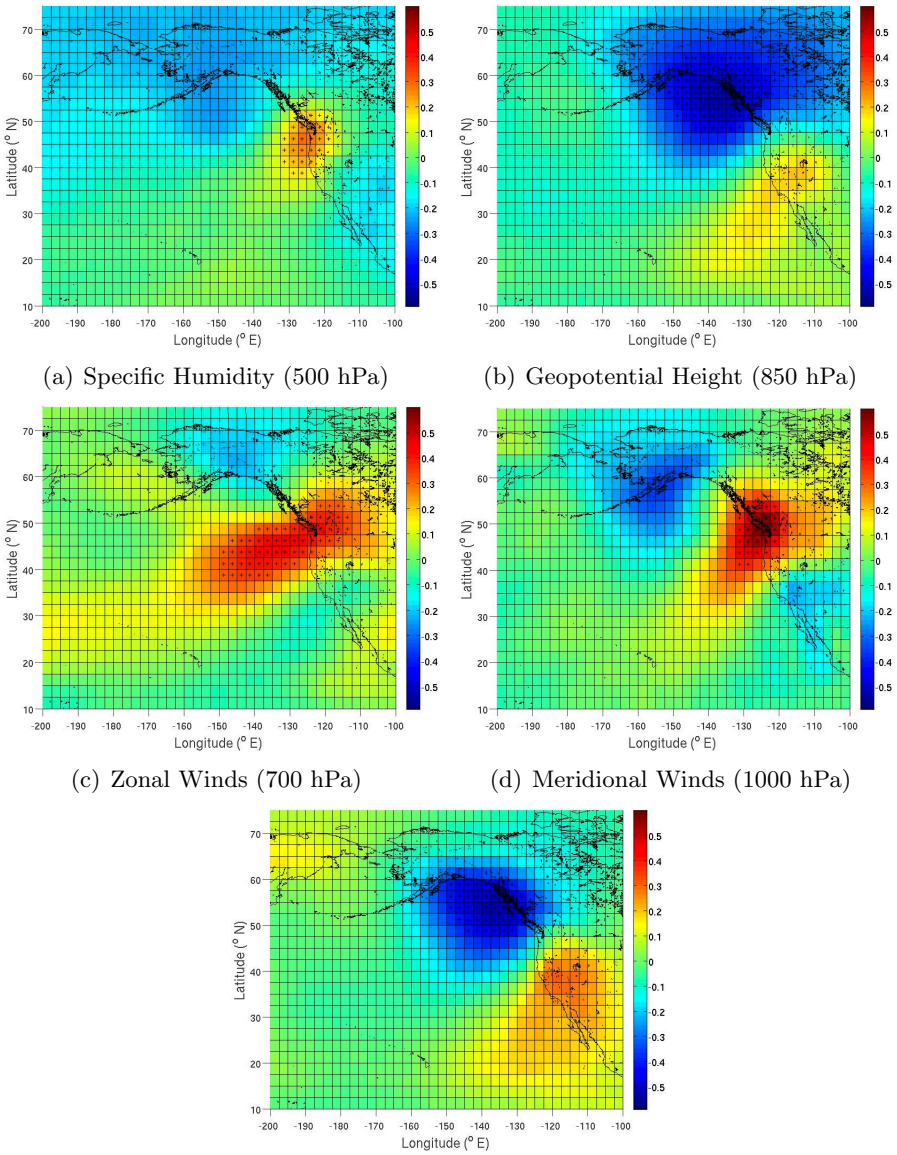

(a) Specific Humidity (500 hPa)

(b) Geopotential Height (850 hPa)

(c) Zonal Winds (700 hPa)

(d) Meridional Winds (1000 hPa)

(e) Mean Sea Level Pressure

Figure 3.3: Correlation maps highlighting the relationships between the selected large-scale predictor variables at individual grid cells and the average precipitation received over Vancouver Island. Large-scale data is obtained from NCEP Reanalysis fields while precipitation observations are derived from Environment Canada weather stations. Black crosses indicate the selected grid cells used for predictors in the downscaling model.

3.2 Synoptic Typing of Precipitation

The observed precipitation dataset is divided into representative precipitation states or types based on the clustering algorithm described in the methodology section, derived from Vrac [Vrac et al. (2007)]. This division is performed in both the split-record and cross-validation approaches to assess the capabilities of the statistical model. Winter types were produced from the first fifteen years of the baseline period while summer types were generated using the last fifteen years. Which division to use was determined by comparing the abilities of both to replicate observations and selecting the superior of the two. Validation was performed using both NCEP circulation data and using predictors taken from the ensemble of climate models under the 20^{th} century climate experiment. The example clusters described below were taken from the split-record validation experiments using data from the NCEP Reanalysis to produce predictor variables.

Following the clustering algorithm of winter precipitation under the split-record separation of the dataset, the precipitation data was grouped into five representative states (Figures 3.4 through 3.8). States one and three describe high intensity precipitation with daily average values reaching over 100 mm. In both of these states the greatest precipitation occurs on the west coast of the island, however the highest values are confined to a few individual stations. In the case of state one the greatest intensities are located on the northern stations, while in state three, the maximum values are on the more southerly stations. The remaining three representative states describe low to moderate intensity precipitation and occur the most frequently. State four shows a pattern of trace precipitation with intensities ranging from 1 to 5 mm and a spatial distribution with the largest values occurring on the northwestern tip of the island with a decreasing gradient towards the east. All of the patterns illustrate the dominance of southwesterly flow during the winter months, as well as highlight the range in precipitation intensities from trace to extreme values.

In the five winter states based on precipitation patterns the five associated circulation patterns display common features, with a prominent Aleutian Low Pressure-Cell in the Gulf of Alaska and strong southwesterly flow west of Vancouver Island (Figures 3.4 through 3.8 (b)). When individual states' climatology are compared against the overall climatological average however, distinct differences between the states begin to emerge. States one and three, the least frequent and associated with the most intense precipitation, have distinct differences in circulation relative to the other three states. State one possesses the strongest

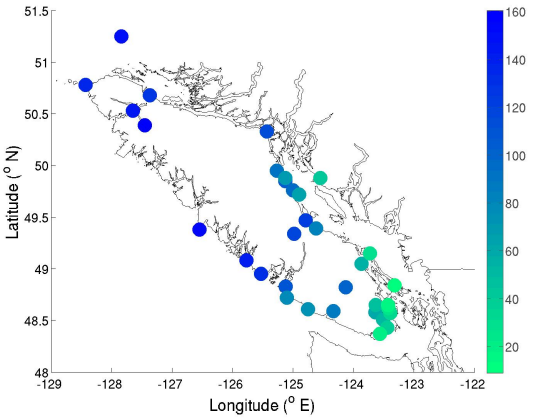

(a) Precipitation State 1

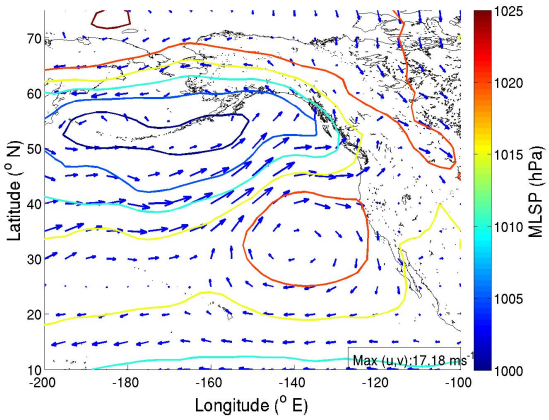

(b) State 1 Circulation Climatology

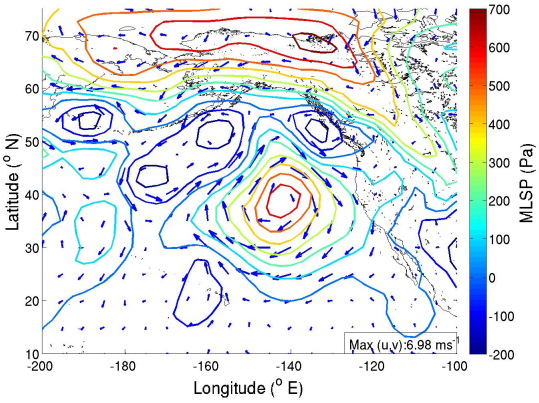

(c) State 1 Circulation Anomaly

Figure 3.4: The first of five synoptic types generated by the clustering algorithm grouping together days of similar precipitation during the winter months. Each precipitation pattern displays the daily average precipitation in each type at each station.The second plot displays the average meridional and zonal wind fields (vectors) combined with average sea level pressure (contours). The third plot displays the circulation anomaly patterns relative to the climatological average over every day from 1971 to 2000. State 1 occurs in 0.89% of the days in the observational record.

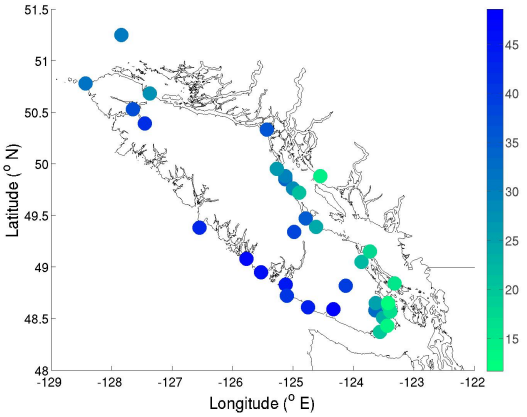

(a) Precipitation State 2

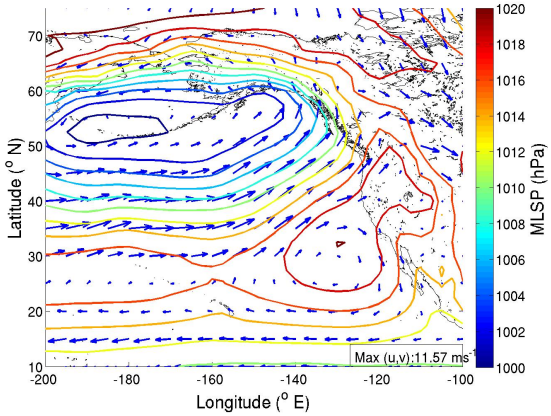

(b) State 2 Circulation Climatology

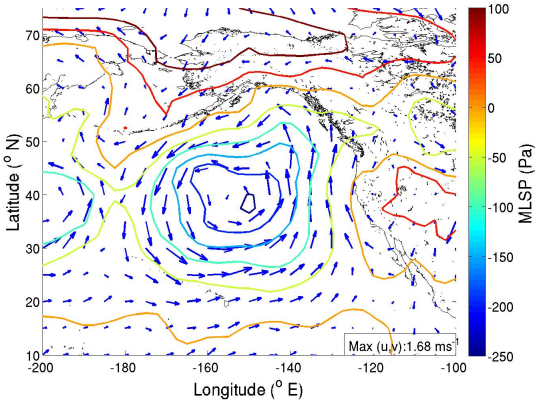

(c) State 2 Circulation Anomaly

Figure 3.5: The second synoptic type. Same layout as the previous figure. State 2 frequency: 14.56%.

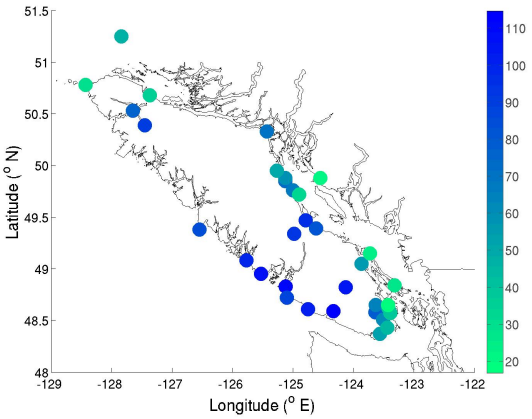

(a) Precipitation State 3

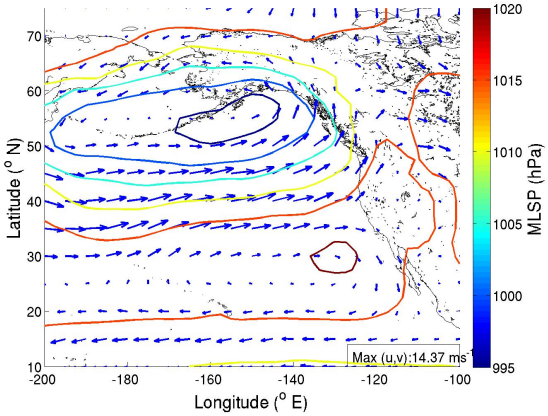

(b) State 3 Circulation Climatology

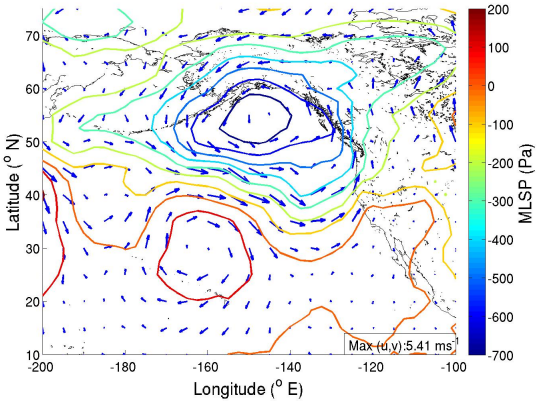

(c) State 3 Circulation Anomaly

Figure 3.6: The third synoptic type. Same layout as the previous figure. State 3 frequency: 2.83%.

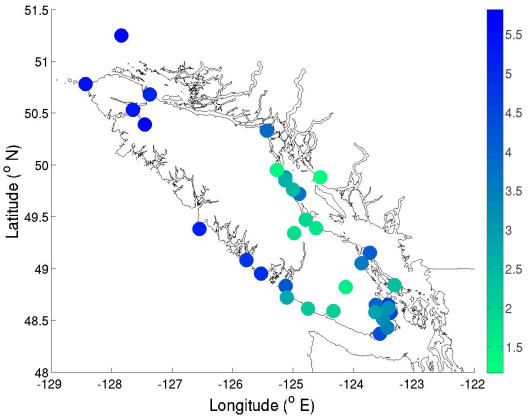

(a) Precipitation State 4

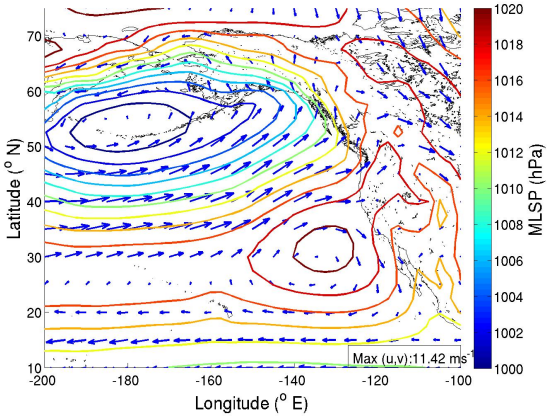

(b) State 4 Circulation Climatology

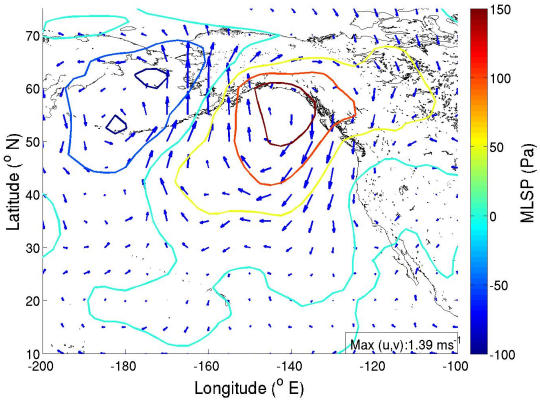

(c) State 4 Circulation Anomaly

Figure 3.7: The fourth synoptic type. Same layout as the previous figure. State 4 frequency: 37.50%.

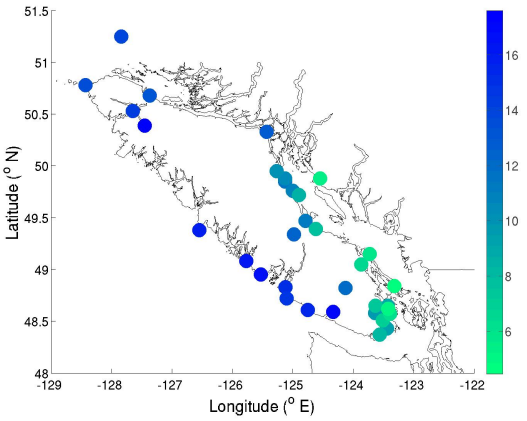

(a) Precipitation State 5

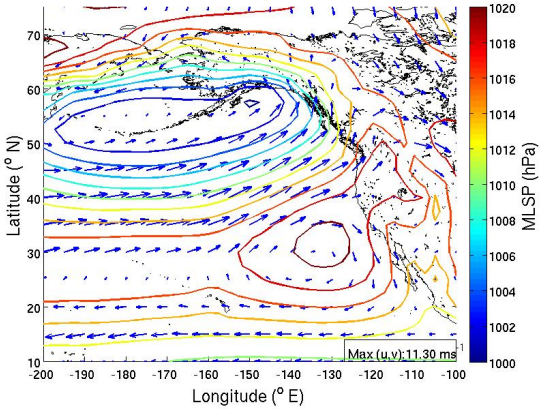

(b) State 5 Circulation Climatology

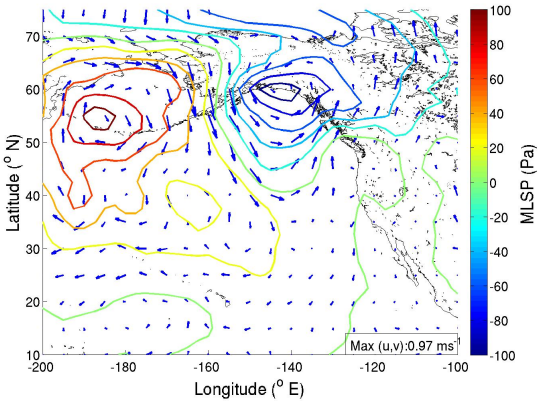

(c) State 5 Circulation Anomaly

Figure 3.8: The last of the five synoptic types generated by the clustering algorithm grouping together days of similar precipitation during the winter months. Same layout as the previous figure. State 5 frequency: 44.22%.

and most northerly North Pacific High resulting in an eastward deflection of the southwesterly flow. In state three, the Aleutian Low is the deepest and the most easterly. States two, three and five display characteristics associated with the 'Pineapple Express', a term describing the advection of moist air from the region surrounding the Hawaiian Island Chain to the North East Pacific coastline that causes significant precipitation [Mass (2008)]. In state four a weak high pressure ridge exists in the circulation anomaly pattern, resulting in northerly airflow along the BC coast and reduced precipitation intensity. Though the average patterns display only subtle differences between them, the circulation anomalies reveal the distinct differences occurring in the atmosphere associated with the different precipitation states (Figures 3.4 through 3.8 (c)).

The characteristic clusters defined for the summer period display similar traits as those during the winter months, with rarely occurring states describing high intensity precipitation and a few low to moderate intensity states that occur much more frequently (Figures 3.9 through 3.13). The state with the lowest magnitudes, state one, occurs the most frequently at 51% of the time. Coupled with the second state, which occurs on 33% of the summer days, 84% of the daily precipitation during the summer months amounts to less that $6.5mm$ of precipitation. This suggests the dominant precipitation occurring in the summer months is that of low intensity rainfall, interspersed with high intensity events such as frontal systems or mid-latitude cyclones (states three and five) [Mass (2008)]. The spatial distribution of the precipitation shows only a minor difference relative to that of the winter months. The shift in prevailing winds to northwesterly during the summer months is represented in the more west to east gradient in precipitation observed in each of the states.

The circulation fields observed in each of the synoptic types for the summer months repeat the form of the results seen in the winter aggregation with characteristic patterns corresponding to each of the different classes of precipitation. The climatology patterns of states three and five display an intense low-pressure cell in the Gulf of Alaska with correspondingly strong cyclonic flow producing southwesterly winds just offshore of Vancouver Island. The dominant states, one and two, present different patterns with significant northwesterly and westerly atmospheric flow, respectively. In both states, a large, a high-pressure centre is present in the region of 30^oN to 40^oN. The first two types, states 1 and 2, are the two most frequently occurring precipitation states and produce the lowest precipitation intensities during the summer season.

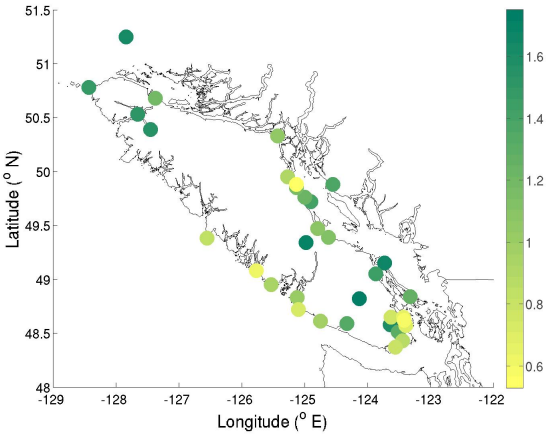

(a) Precipitation State 1

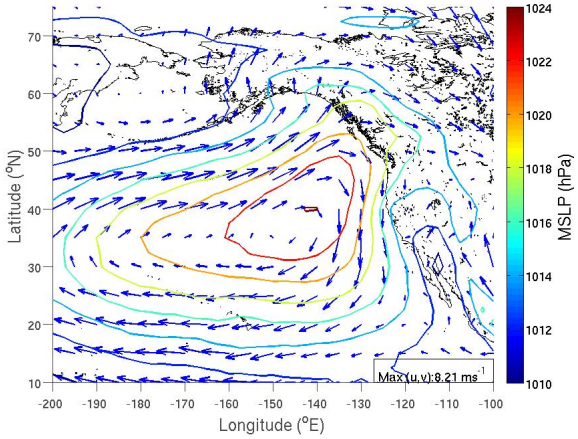

(b) State 1 Circulation Climatology

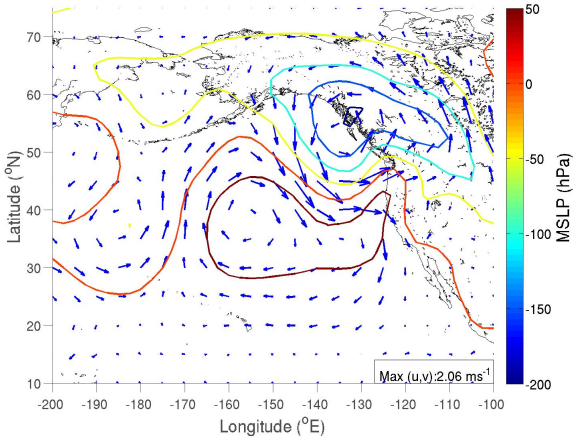

(c) State 1 Circulation Anomaly

Figure 3.9: The first of five synoptic types generated during the summer months. Same format as in the winter states. State 1 frequency: 51.11%.

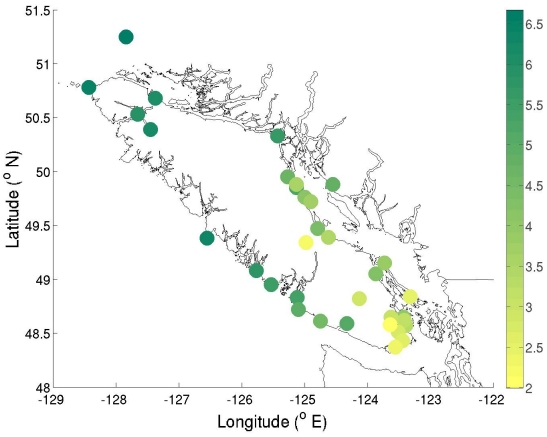

(a) Precipitation State 2

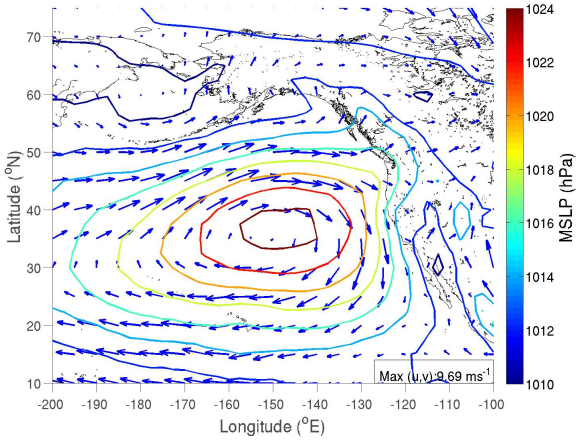

(b) State 2 Circulation Climatology

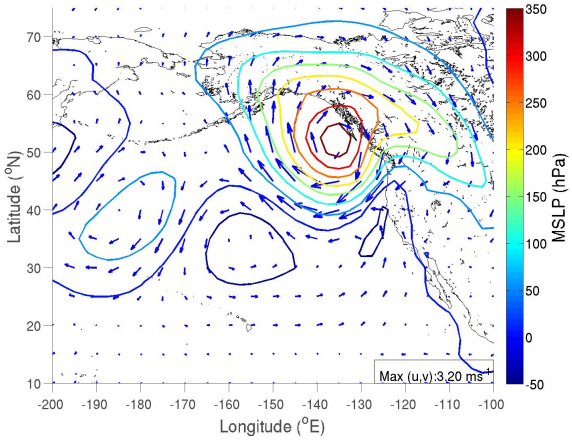

(c) State 2 Circulation Anomaly

Figure 3.10: The second synoptic type. Same format as in the winter states. State 2 frequency: 33.05%.

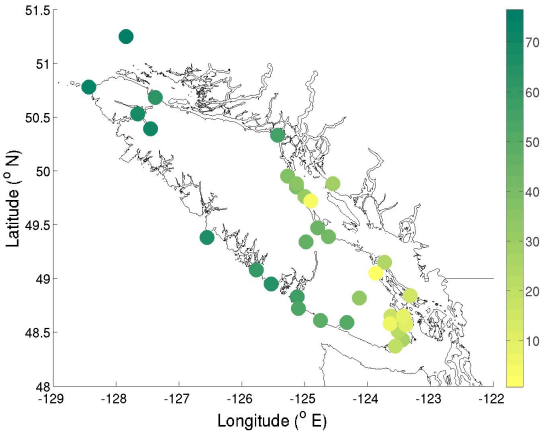

(a) Precipitation State 3

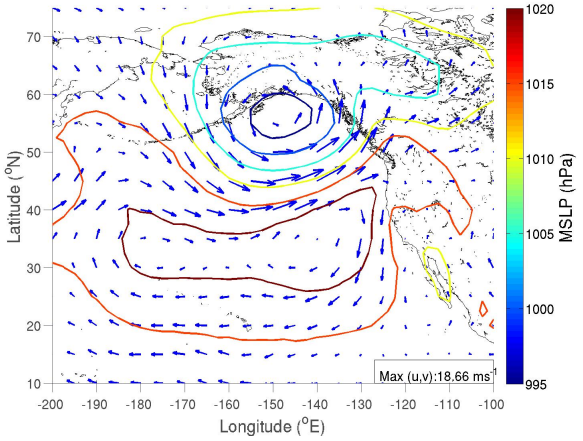

(b) State 3 Circulation Climatology

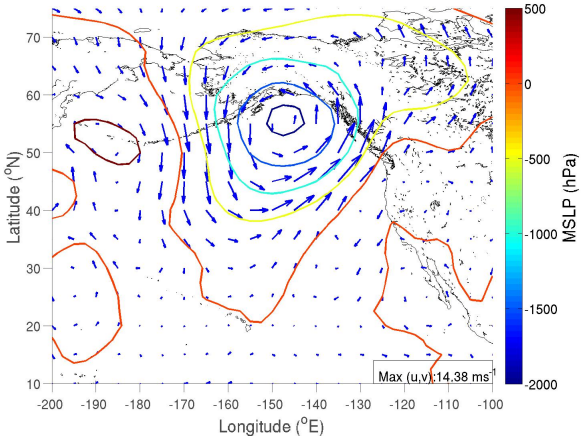

(c) State 3 Circulation Climatology

Figure 3.11: The third synoptic type. Same layout as the previous figure. State 3 frequency: 0.56%.

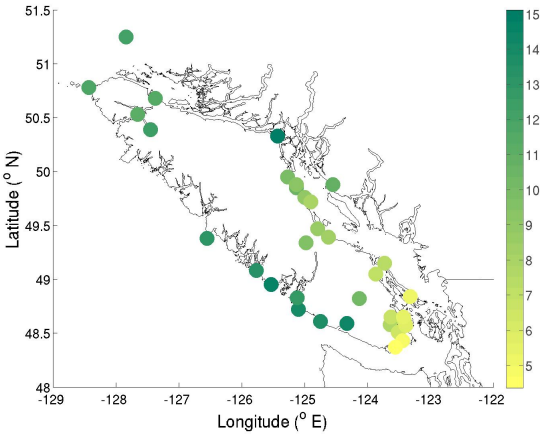

(a) Precipitation State 4

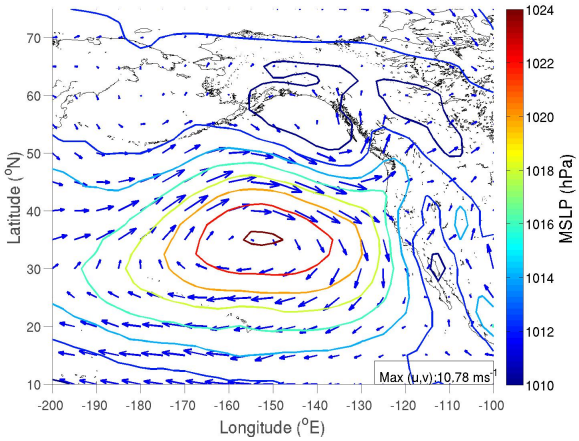

(b) State 4 Circulation Climatology

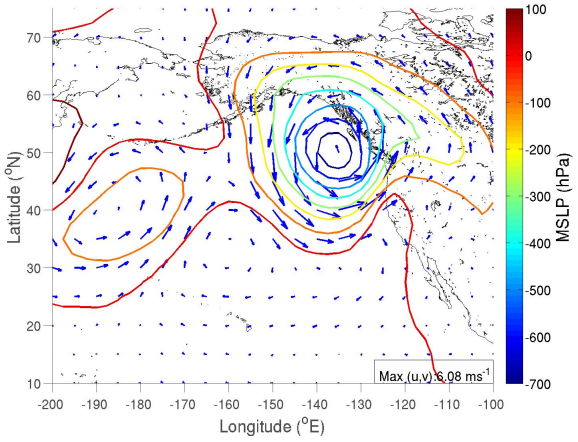

(c) State 4 Circulation Anomaly

Figure 3.12: The fourth synoptic type. Same layout as the previous figure. State 4 frequency: 13.21%.

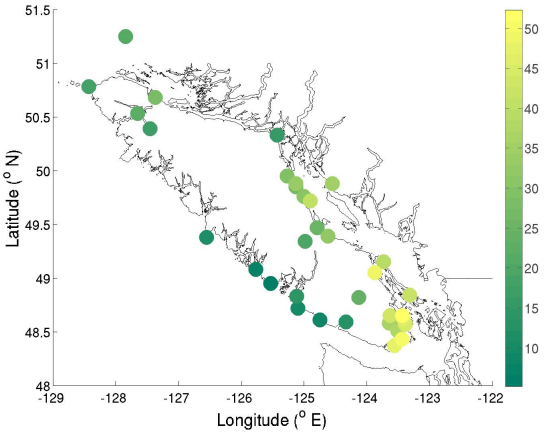

(a) Precipitation State 5

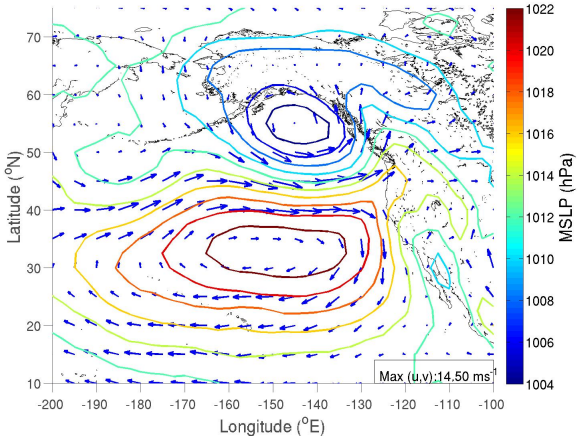

(b) State 5 Circulation Climatology

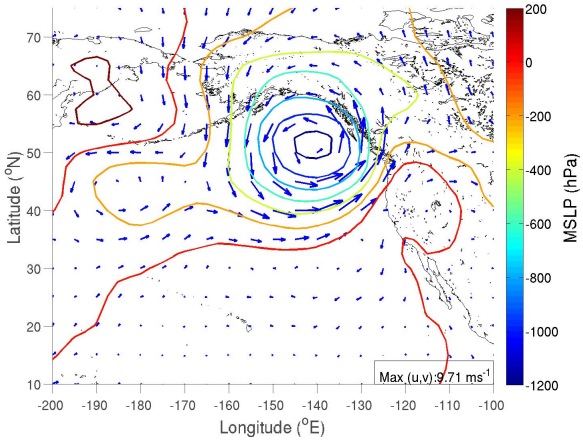

(c) State 5 Circulation Anomaly

Figure 3.13: The fifth synoptic type. Same layout as the previous figure. State 5 frequency: 2.10%.

Under the cross-validation subdivision of the precipitation dataset, the clustering algorithm is employed multiple times in each of the different 25-year subsets of the data used to train the statistical model. The resulting patterns obtained possess similar fields as in the figures above, however the number of synoptic types obtained by the clustering method varies slightly from set to set. Depending on which subset is used, there are four to seven representative states established by the algorithm due to variations in the seasonal precipitation amounts on the island. In the case of common clusters synoptic types are chosen using the split-record approach, while common EOFs were evaluated using the cross-validation approach. The precipitation patterns are clustered as before yielding the same types as displayed above, however in these cases the large-scale circulation patterns are taken from either the concatenated predictor variables (common clusters), or the principal components of the common Empirical Orthogonal Functions. The identified states are then applied to the validation period to test the capabilities of the different variations of the statistical downscaling model.

3.3 Climate Model Circulation

To determine what shifts in precipitation are likely to be produced by downscaling, the trends in atmospheric circulation patterns (which influence the statistical model simulating precipitation) are examined in terms of differences in the thirty-year average from the end of the twentieth century to twenty-year average from the end of the twenty-first century. The projected patterns (Figure 3.14) are derived from the ensemble of the four climate models under the SRES A2 Emissions Scenario. The winter months (NDJF) are marked by a north-northwesterly shift in the position of the Aleutian Low with an associated deepening of its central pressure level by as much as 600 Pa. Average wind speeds in the cyclonic flow around the low is enhanced by as much as 3 m/s and the westerly storm track (defined by MSLP contours beginning at 40^oN at the western boundary of the Northeast Pacific) is shifted northward by three to five degrees towards the Aleutian Islands (Figure 3.14, top row). Over Vancouver Island, the southwesterly winds exhibit a slight weakening, however the magnitude of changes in the wind field across the entire British Columbian coastline is lower than is seen in the broader area of the Northeast Pacific Ocean. In the summer months (JJAS) there is a minor (1^o to 2^o) northward shift of the North Pacific High with a simultaneous strengthening of the anti-cyclonic winds that accompany it. In this case the differences in the pressure field are small (50 to 100 Pa), however the changes in the winds act to strengthen the seasonal northwesterly winds that occur during the summer months

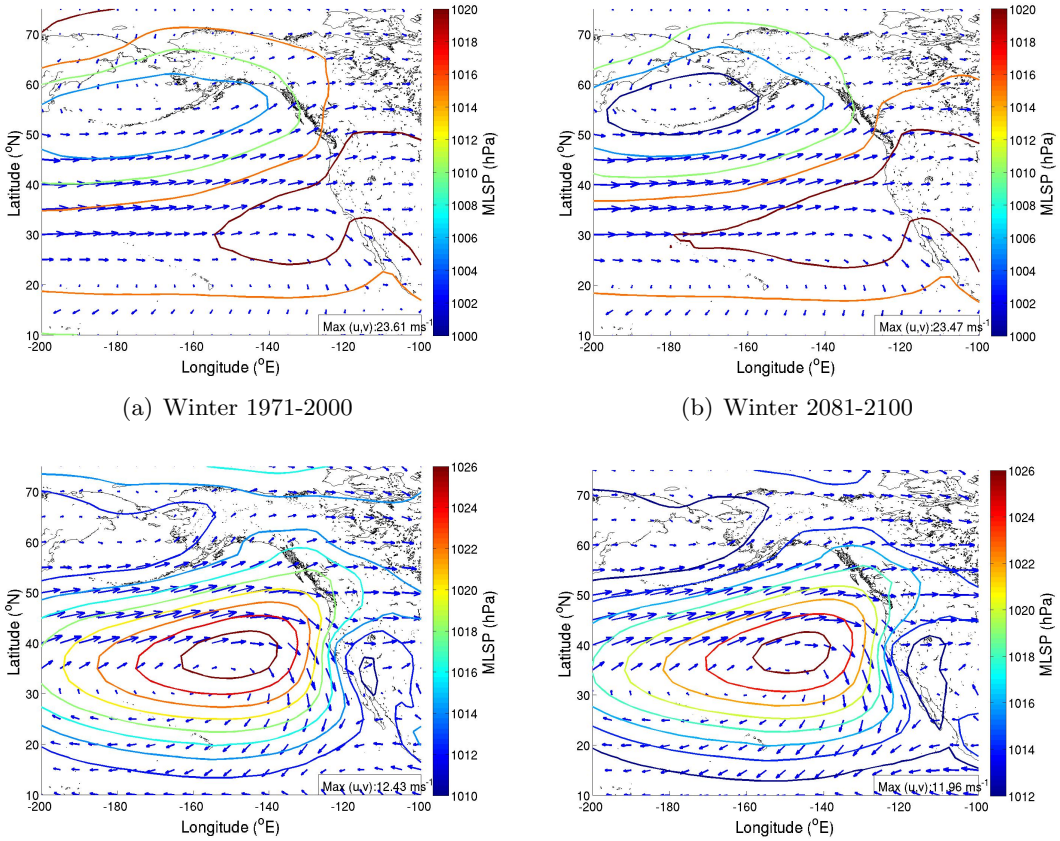

(a) Winter 1971-2000

(b) Winter 2081-2100

(c) Summer 1971-2000

(d) Summer 2081-2100

Figure 3.14: Average plots of MSLP (contours), meridional and zonal winds taken from climate model output in both the winter and summer seasons during the 1971-2000 baseline and the end of the 21st century. Top row: Winter 1971-2000 and 2081-2100; Bottom Row: Summer 1971-2000 and 2081-2100.

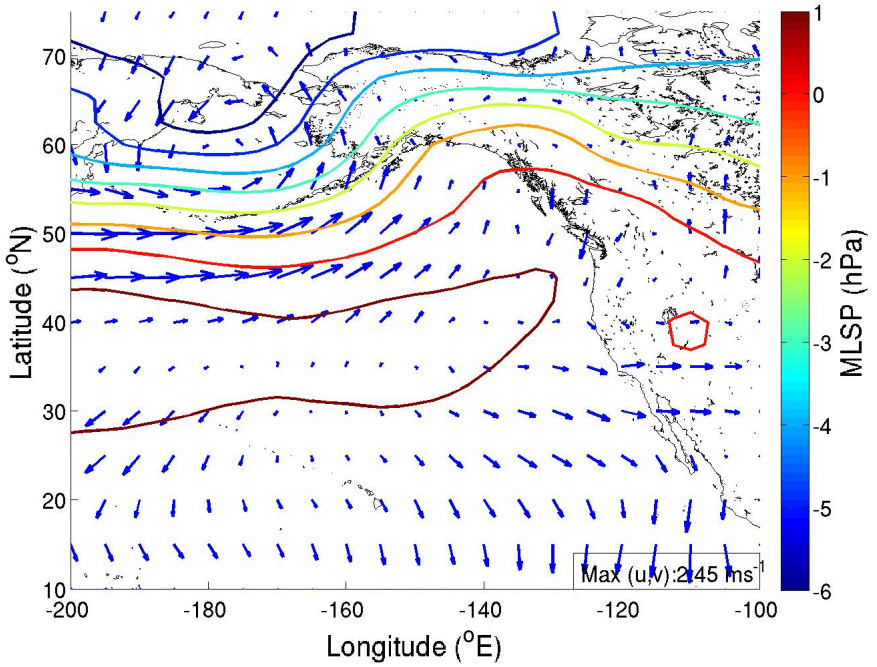

(a) Winter Difference Map

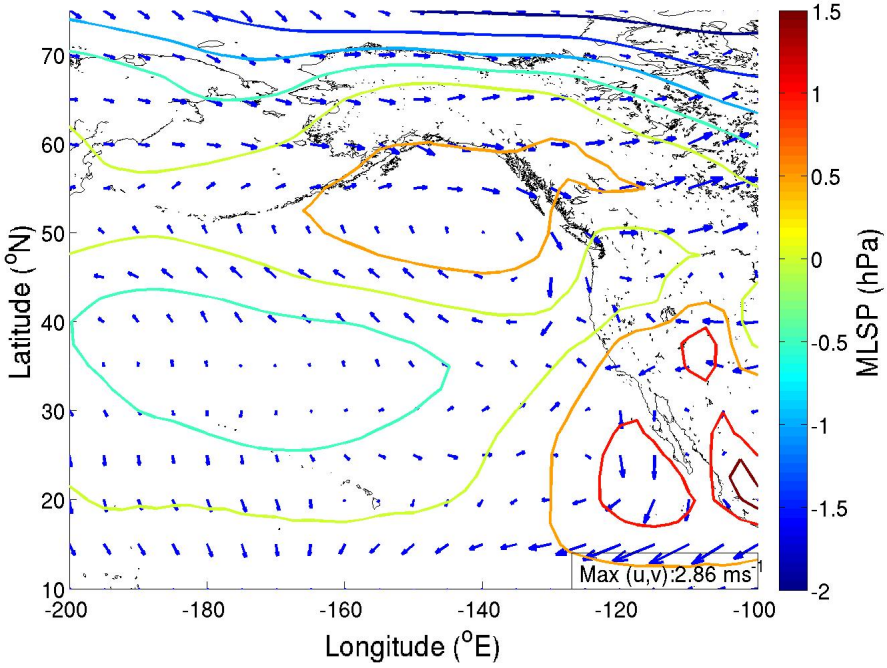

(b) Summer Difference Map

Figure 3.15: Difference plots of MSLP, meridional and zonal winds in both winter and summer seasons between the end of the 21st century and the 1971-2000 baseline. The maps highlight the projected shifts in both the semi-permanent pressure cells and the winds patterns.

by up to 2 m/s (Figure 3.15). This effectively acts to enhance the preexisting patterns in the circulation during the summer months. Both seasons' projected differences match those obtained by previous studies examining future winds and SLP over the Northeast Pacific Ocean [Merryfield et al. (2009); Salathe (2006)].

3.4 Synoptic Typing of Precipitation: Validation

The results of applying the downscaling model to the projection period are plotted as percent anomalies relative to the selected baseline time period. Comparisons are made between the climatologies of the individual stations, meaning the averages of projected daily precipitation values during the future periods are compared against the averages of the observed daily precipitation values from the historical baseline. The downscaling model is trained in each case by developing atmospheric composites using NCEP circulation variables. Validation is performed by simulating a subset of the observational period and comparing the simulated data to observations. The simulated data is produced by the downscaling model, employing predictors taken from both NCEP Reanalysis and large-scale climate model data (from the Climate of the 20^{th} century experiment). Coloured circles represent the precipitation anomalies, with blue signifying a positive change and red describing a negative change. The magnitude of the differences is defined with respect to the reference circle in each of the figures (set at 10% change). In the simulated values, the green cross within the circles represents a percent change that is statistically significant at the 5% significance level. Absolute values of the validation experiments are also provided (Table 3.4) for the four representative stations for comparison.

Simulated data driven by predictors from NCEP Reanalysis present better agreement with 20^{th} century observations than simulations produced from predictors obtained from climate model simulations. The closer agreement is not unexpected given the possible phase differences in the various climate model projections compared to the large-scale circulation represented by the NCEP data. As a result, in each of the validation experiment types (split-record or cross-validation) the NCEP based predictors produce simulated data that is closer to observations than those produced using predictors from the climate models. The spatial patterns seen in the validations performed using climate model data are largely the same as those driven by NCEP data, however.

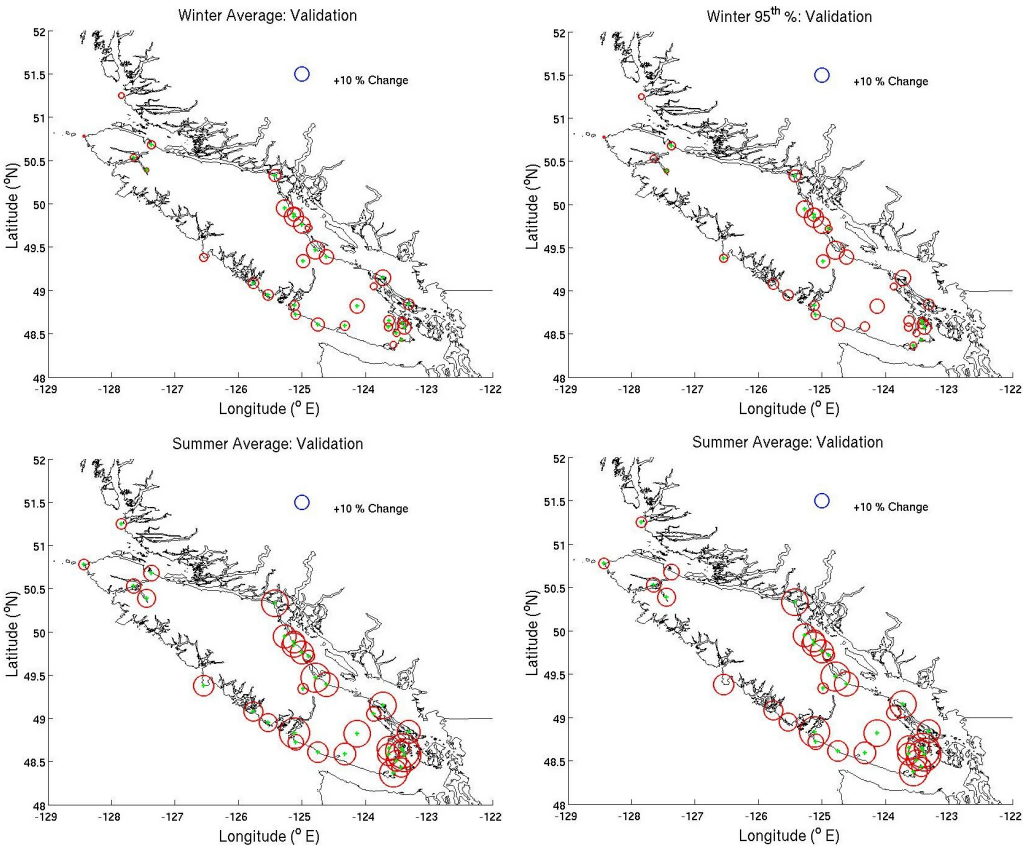

Figure 3.16: Validations of the synoptic typing statistical model for winter (top row) and summer (bottom row), evaluating both averages (left column) and extremes (right column) of precipitation. Simulated data is obtained from the NCEP Reanalysis data under the split-record dataset division. Blue circles denote a positive change, while red circles denote a negative change.

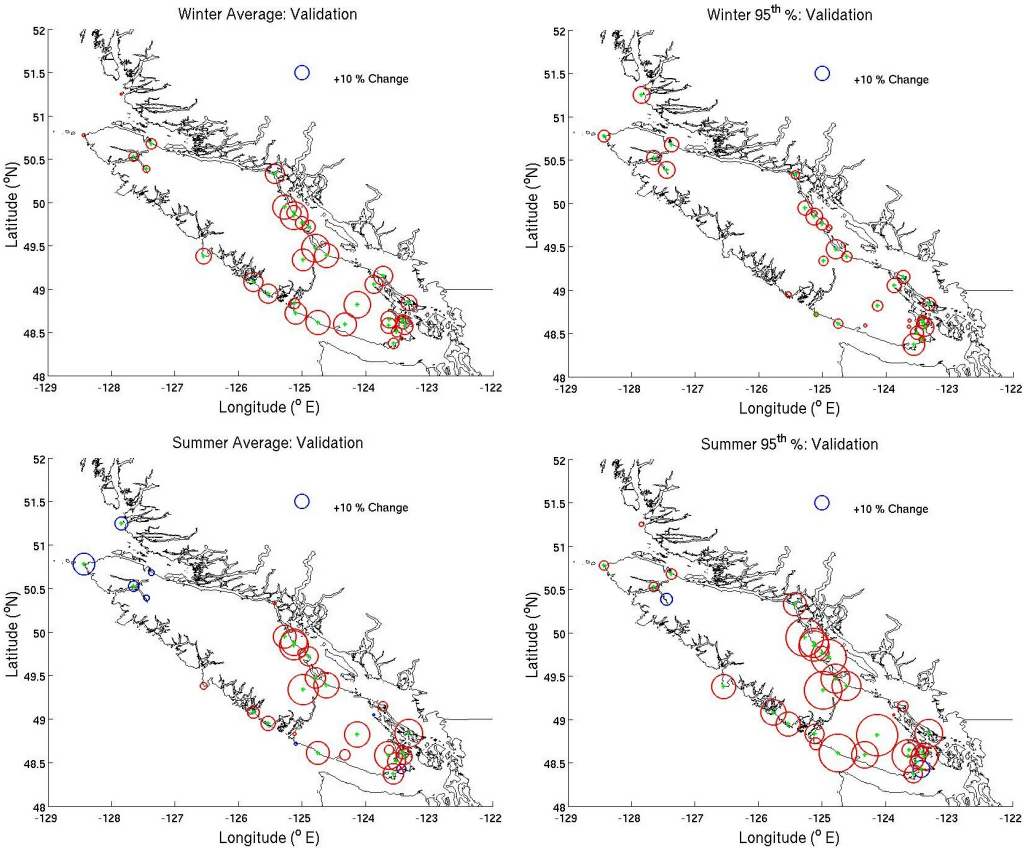

Figure 3.17: Validations of the synoptic typing statistical model under the split-record approach using predictors derived from the ensemble of climate models. Same layout as previous figure.

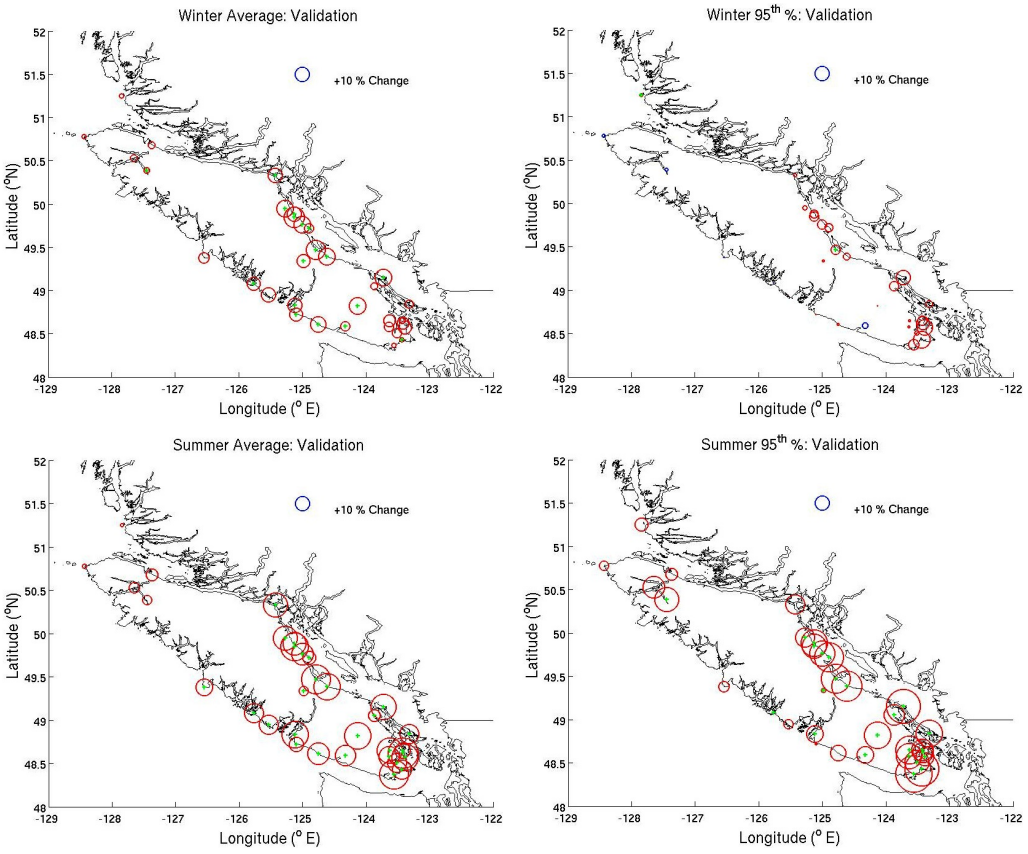

Figure 3.18: Validation of the downscaling model using predictors derived from NCEP Reanalysis data under the cross-validation approach. Layout is the same as in the previous figure.

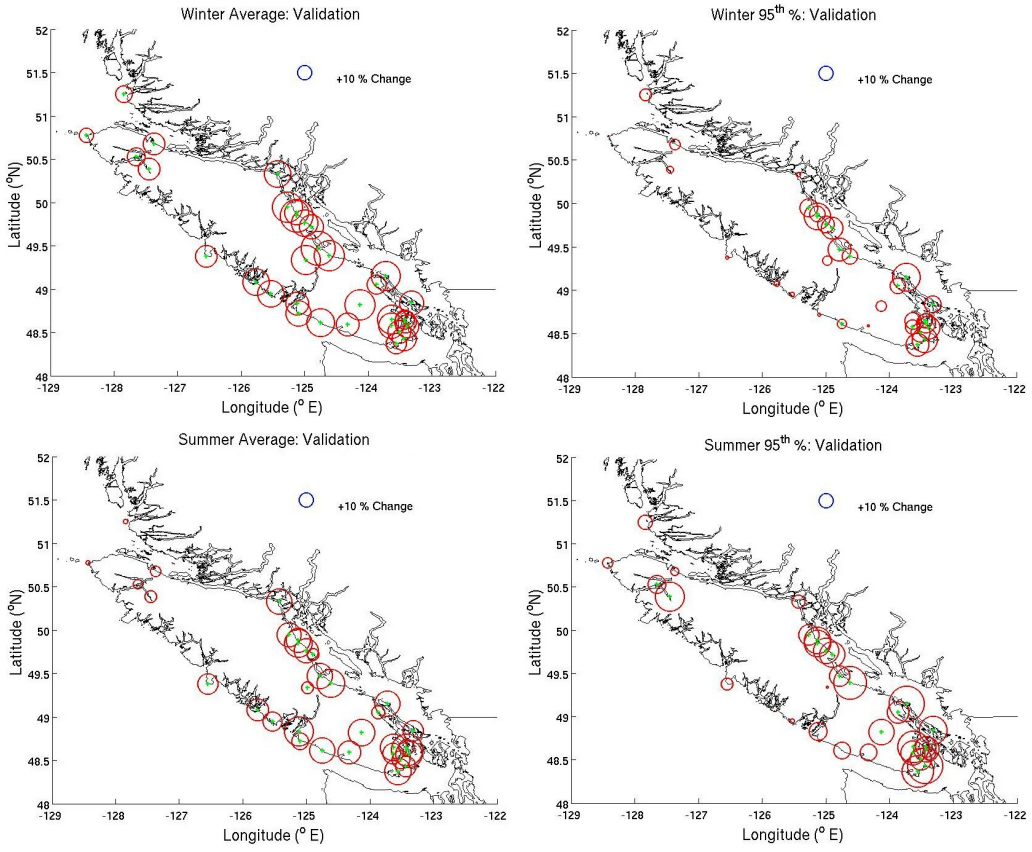

Figure 3.19: Validation of the downscaling model using the cross-validation data divisions with predictors derived from an ensemble climate models' data. Layout is the same as in the previous figure.

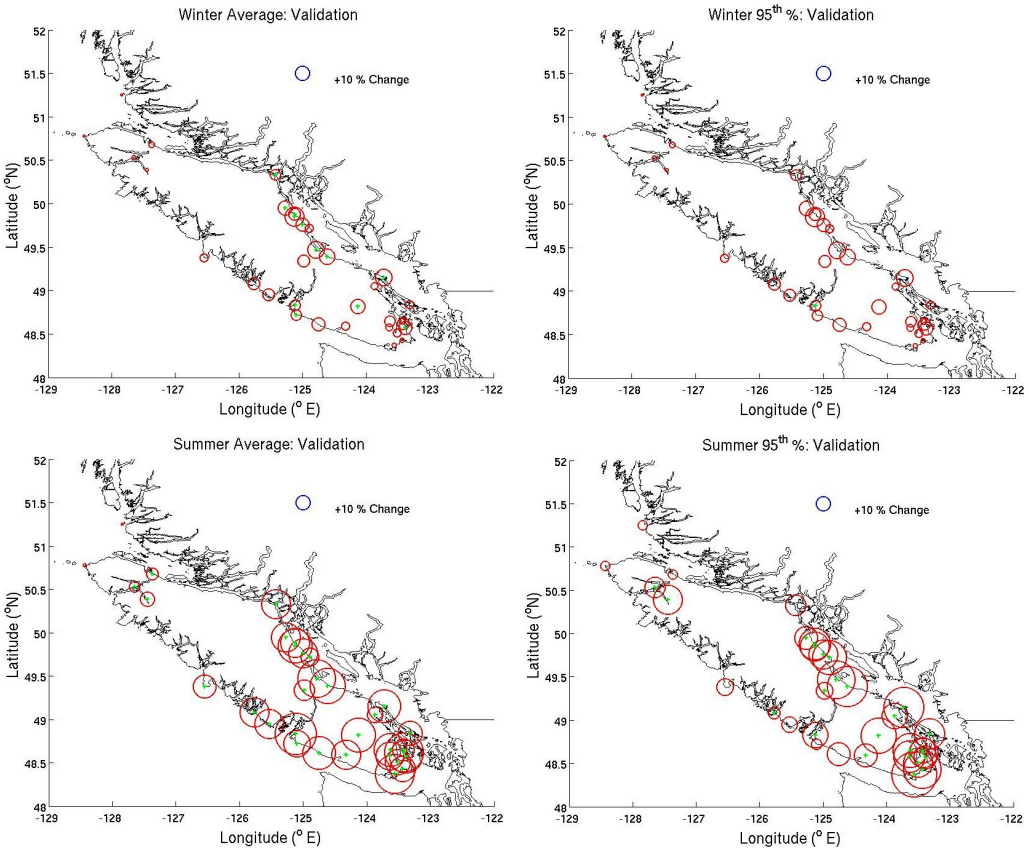

Figure 3.20: Validation of the downscaling model using predictors derived from principal components of the common EOFs (based on NCEP data). Layout is the same as in the previous figure.

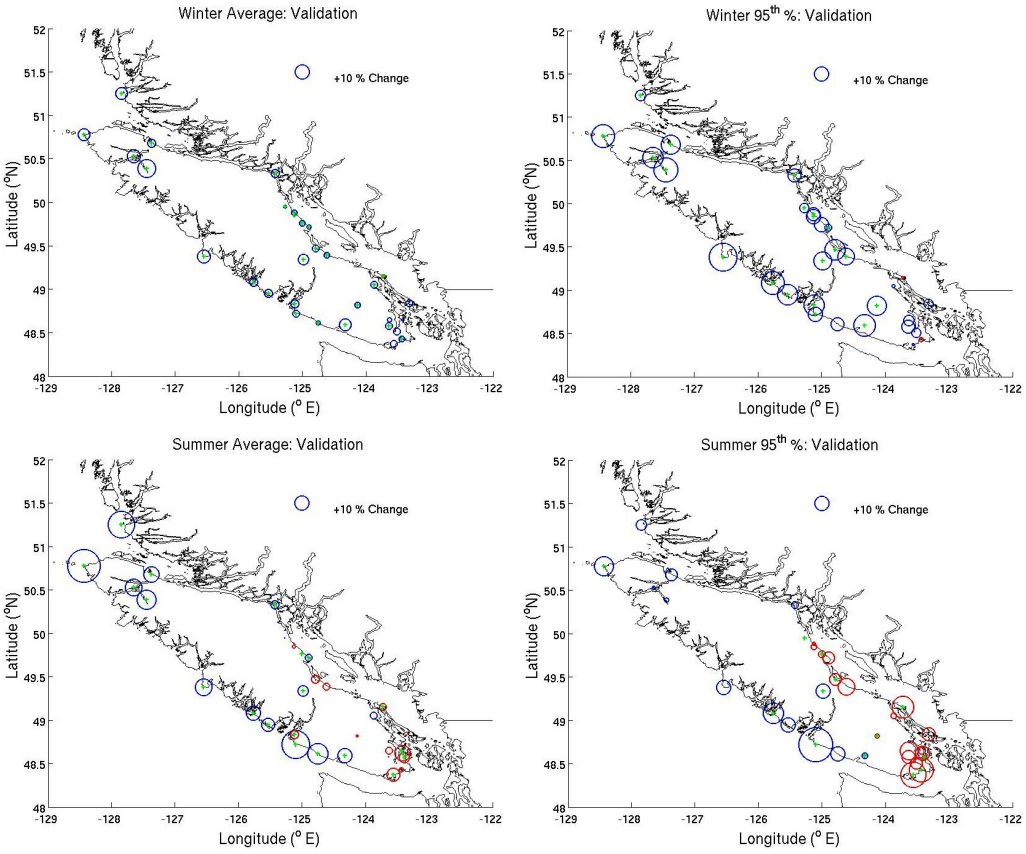

Figure 3.21: Validation of the downscaling model using predictors derived from principal components of the common EOFs (based on the ensemble of climate model data). Layout is the same as in the previous figure.

The results of the winter season validation experiments for the model ensemble, driven by averaged predictor values, reveal a dry bias (red circles) at all of the examined stations with a maximum of 19% underestimate of mean precipitation and 14% underestimate of extreme (95^{th} percentile) precipitation (Figure 3.17). The bias is greater on the southeastern half of the island in the case of mean precipitation and relatively uniform for extreme values, though stations on the west coast show relatively good agreement with the observations in the case of extreme values. In the summer season, the validation again presents with a west to east gradient in the magnitude of the bias with an overestimation of precipitation intensity on the northern tip and an underestimation elsewhere. In this case the dry bias on the southern regions is larger than in the winter season with simulated precipitation underestimated by upwards of 20% for the extreme values. Additionally, the extreme precipitation appears to be less well represented in the summer months compared to the winter months, with a dry bias of 5% to 10% greater than that of the winter season.

Dry biases are also present in the validations conducted using both the cross-validation and common clustering approaches, with lower than expected precipitation seen in both the summer and winter months for both average and extreme values (Figure 3.19). The cross-validation simulation averages are relatively uniform across the island, with values mostly around 10% lower than expected by the observed climatology. The common clustering results are more like those of the split-record validation with slightly greater (0% to 4% more) underestimation in both seasons. Extreme precipitation anomalies of both methods show a strong spatial dependence with stations along the western and northern halves of the island possessing negligible differences between the simulated values and observation. A dry bias still exists along the eastern coast however, from Campbell River Airport to the north stretching south to the Sooke Harbour Basin. Employing the two approaches during the summer months yields more effective simulations than in the case of the split-record validation. A slightly lower dry bias is present with better representation on the southern part of the island. The majority of stations possess simulated average and extreme precipitation with values underestimated by 15% compared to observations.

In contrast to the validations conducted from predictors based on the ensemble mean values, the results of the common EOF predictors reveal dry biases when supplied with NCEP data (Figure 3.20), and mixed results when predictors are taken from climate model data (Figure 3.21). Simulated precipitation generated by NCEP-based predictors deliver results that are largely the same as those seen in the other validation results. The model derived results display unique trends with both wet and dry biases. The model-based, simulated

winter averages agree well with observations at most island stations, with closer matches seen on the eastern coast. The downscaling model overestimates winter extreme precipitation by 10% to 15% at weather stations outside of the southern tip of the island. Simulated precipitation during the summer months using the common EOF predictors presents contrasting anomalies, with a wet bias observed on the western coast and a dry bias seen on the southeastern coast. The same pattern occurs for both average and extreme precipitation values, with the extreme anomalies being 5% to 10% larger than the averages anomalies. The dramatically different validation results, produced using common EOF predictors, highlight the sensitivity of the downscaling model to the influence of the large-scale atmospheric variables, to the form of the predictor variables employed, and to the region from which these predictors were obtained.

3.5 Synoptic Typing of Precipitation: Future Projections

Future precipitation statistics are determined using the downscaling model employing the influence of atmospheric circulation values projected by the climate models. In the case of predictors taken from the grid cell averages, projections are evaluated from an ensemble of the selected models (applying the split-record and cross-validation divisions to compare different training periods and bias corrections), and using the common clustering approach. Common EOFs are trained and bias corrected under the cross-validation data division and the results of the individual models are combined after the fact in an ensemble as well. Both winter and summer projections are corrected at each station individually for the bias identified in the validation experiments described previously.

Winter precipitation projections under the grid cell averages, split-record bias correction approach are almost uniformly positive, with average precipitation changes ranging from -2% up to $+14\%$ and the majority of stations experiencing a 5% increase (Figure 3.22). Extreme precipitation (95^{th} percentiles) follows a similar pattern, with a wider range of values from -6% to $+15\%$ and an expected difference of $+6\%$. In both average and extreme precipitation, there are not any strong spatial trends or regional differences in the magnitude of the projections other than a prevalence of larger magnitudes of change on the northern two-thirds of the island relative to the southern portion. Conversely, summer precipitation projections are almost all uniformly negative with future rainfall expected to range from a decrease of 15% to an increase of 2%, though only the largest of these values are statistically

Winter Months Validation				
	Ensemble Average		Cross-validation	
Stations	Mean	$95^{th}\%$	Mean	$95^{th}\%$
CS	-0.26 ± 0.41	-2.24 ± 1.45	-1.04 ± 0.95	-0.46 ± 4.15
CRA	-1.15 ± 0.29	-2.99 ± 1.59	-1.37 ± 0.57	-3.56 ± 2.84
EP	-1.53 ± 0.46	-0.52 ± 2.34	-2.06 ± 0.98	-1.49 ± 4.06
VIA	-0.23 ± 0.19	-1.56 ± 0.94	-0.58 ± 0.29	-1.97 ± 1.36
	Common EOFs		Common Clusters	
Stations	Mean	$95^{th}\%$	Mean	$95^{th}\%$
CS	0.31 ± 0.25	1.54 ± 0.89	-0.90 ± 0.33	-2.11 ± 1.35
CRA	0.12 ± 0.93	1.32 ± 1.27	-1.32 ± 0.34	-3.06 ± 1.37
EP	0.95 ± 0.76	1.59 ± 1.16	-1.97 ± 0.56	-3.02 ± 2.26
VIA	0.27 ± 0.63	0.30 ± 1.96	-0.69 ± 0.18	-3.11 ± 1.11
Summer Months Validation				
	Ensemble Average		Cross-validation	
Stations	Mean	$95^{th}\%$	Mean	$95^{th}\%$
CS	0.49 ± 0.18	-1.23 ± 0.87	-0.78 ± 0.45	-4.54 ± 2.16
CRA	-0.27 ± 0.13	-2.76 ± 0.72	-0.54 ± 0.27	-3.31 ± 1.56
EP	-0.19 ± 0.29	-3.56 ± 1.60	-1.27 ± 0.55	-8.98 ± 3.39
VIA	-0.01 ± 0.07	-0.40 ± 0.50	-0.30 ± 0.12	-2.05 ± 0.92
	Common EOFs		Common Clusters	
Stations	Mean	$95^{th}\%$	Mean	$95^{th}\%$
CS	0.61 ± 0.57	1.49 ± 1.41	0.47 ± 0.28	-1.11 ± 1.33
CRA	0.14 ± 0.33	0.2 ± 0.60	-0.31 ± 0.10	-3.01 ± 0.55
EP	1.11 ± 0.79	3.32 ± 2.48	-0.12 ± 0.30	-3.47 ± 1.63
VIA	-0.56 ± 0.21	-1.41 ± 1.26	-0.02 ± 0.07	-0.46 ± 0.41

Table 3.1: Absolute difference (mm/day) in precipitation averages at the four representative stations between the observations and the downscaling model simulations for the four prediction methods based on predictors from climate model data.

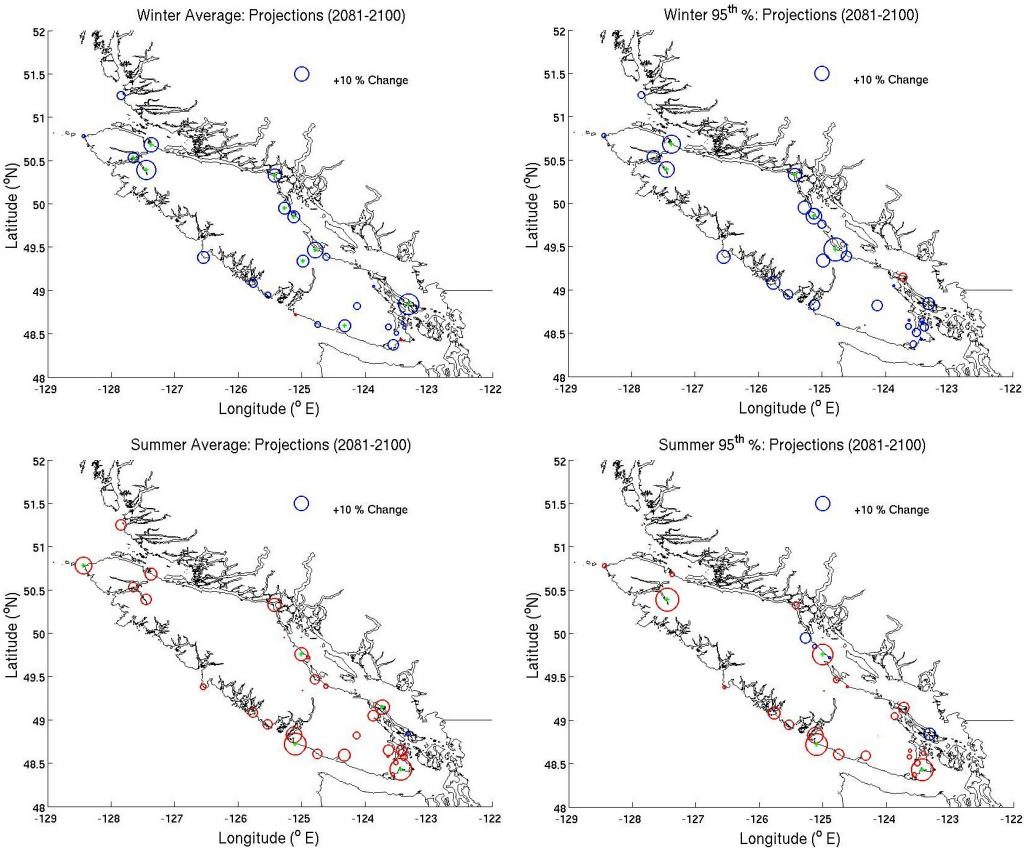

Figure 3.22: Projections of winter and summer, average and extreme precipitation. Future values are obtained from the statistical model driven by averages of the climate model grid cells trained and corrected using the split-record data division. The values are determined from an ensemble average of the four climate model outputs.

significant. Average and extreme precipitation decreases change significantly only at a few relatively isolated stations located on the coast of the island.

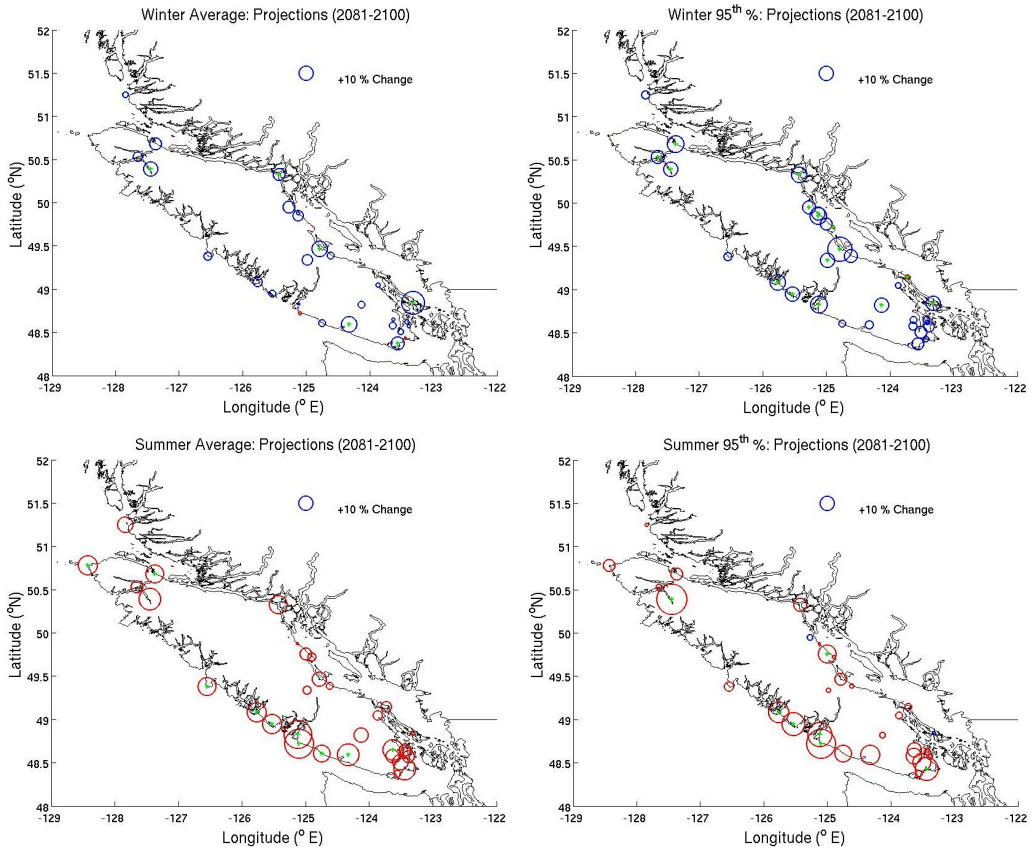

Figure 3.23: Same as the previous figure, only the predictors are derived from a concatenation of the different models' output ("common clustering") before use by the downscaling model.

Patterns similar to those seen in the ensemble averages are repeated in the common clustering approach, which displays almost identical projections in winter and similar projections in summer (Figure 3.23). During the winter season, the only differences between the two methods are very subtle variations among the individual stations' positive precipitation anomalies. In the case of winter extreme precipitation, common cluster values are more consistent with most stations increasing by 7% to 10%, rather than larger increases at a few stations. The spatial patterns in both methods are effectively identical in both average and extreme precipitation. In the summer months, the common clustering, projected decreases in precipitation display a more significant difference at a greater number of stations, with the negative anomalies reaching 20% below the 20^{th} century baseline. The spatial patterns seen in both the average and extreme precipitation also show significant declines on the west coast of the island, as well as at certain stations in the north and south.

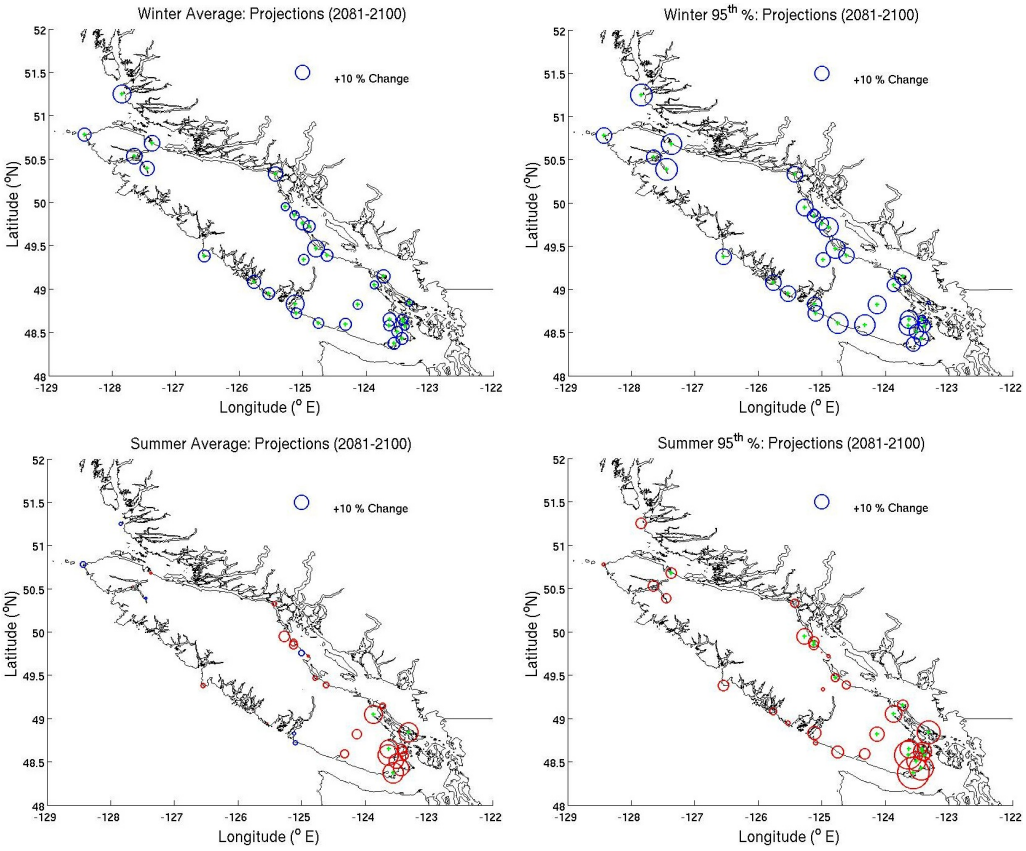

Figure 3.24: Same as previous figure, only the model is trained and bias corrected using the cross-validation separation of the datasets.

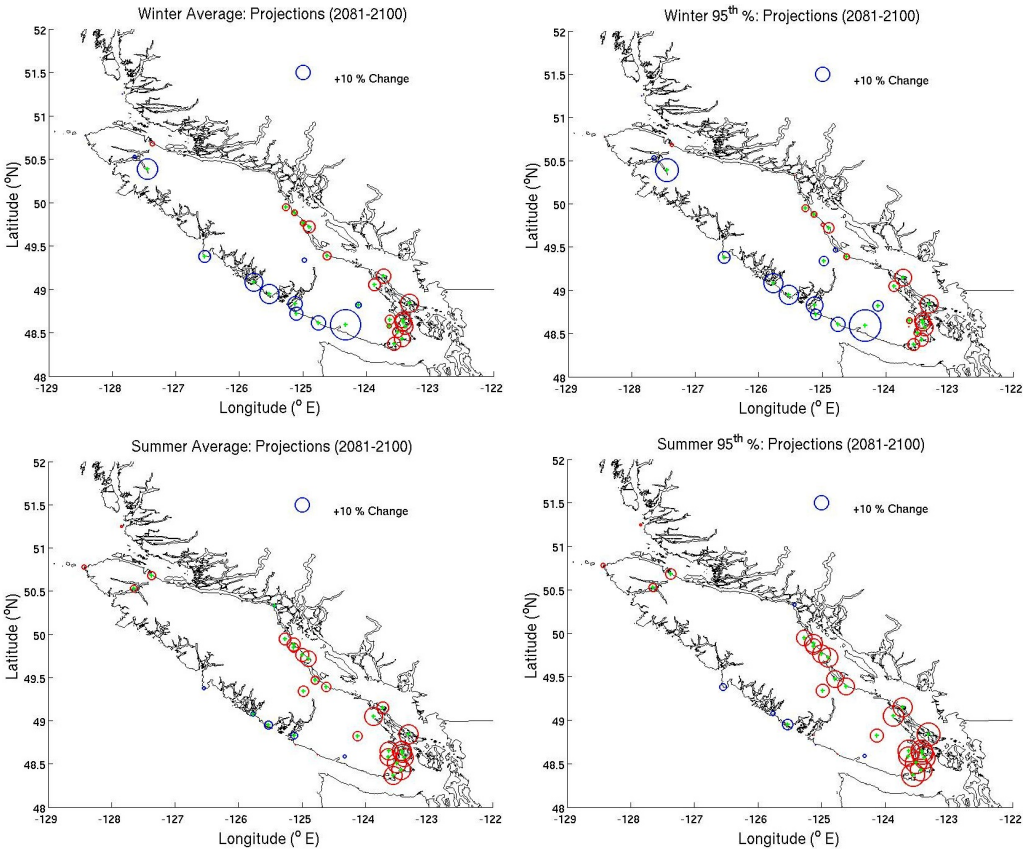

Figure 3.25: Same as previous figures only with predictors taken from the common EOF decomposition of the selected large-scale atmospheric variables

Winter Months Projections				
	Ensemble Average		Cross-validation	
Stations	Mean	$95^{th}\%$	Mean	$95^{th}\%$
CS	0.30 ± 0.36	0.94 ± 1.21	0.87 ± 0.79	3.42 ± 2.88
CRA	0.55 ± 0.26	2.25 ± 1.27	0.34 ± 0.38	2.81 ± 1.86
EP	1.10 ± 0.60	4.32 ± 2.95	1.03 ± 0.70	4.50 ± 2.47
VIA	0.06 ± 0.18	0.57 ± 0.70	0.28 ± 0.22	0.80 ± 0.97
	Common EOFs		Common Clusters	
Stations	Mean	$95^{th}\%$	Mean	$95^{th}\%$
CS	0.71 ± 0.57	0.22 ± 0.62	0.04 ± 0.37	0.07 ± 1.27
CRA	-0.16 ± 0.40	-0.21 ± 0.61	0.43 ± 0.30	1.36 ± 1.16
EP	1.43 ± 0.96	2.28 ± 1.99	0.85 ± 0.51	2.58 ± 2.21
VIA	-0.35 ± 0.22	-0.77 ± 0.64	0.07 ± 0.17	0.83 ± 0.87
Summer Months Projections				
	Ensemble Average		Cross-validation	
Stations	Mean	$95^{th}\%$	Mean	$95^{th}\%$
CS	-0.44 ± 0.20	-0.95 ± 0.82	0.22 ± 0.50	-0.10 ± 1.96
CRA	-0.01 ± 0.09	0.64 ± 0.90	-0.11 ± 0.11	-0.87 ± 0.50
EP	-0.18 ± 0.20	-0.81 ± 1.18	-0.11 ± 0.35	-1.20 ± 1.86
VIA	-0.06 ± 0.06	-0.07 ± 0.31	-0.05 ± 0.08	-0.28 ± 0.51
	Common EOFs		Common Clusters	
Stations	Mean	$95^{th}\%$	Mean	$95^{th}\%$
CS	-0.59 ± 0.56	-0.56 ± 0.98	-0.49 ± 0.22	-1.21 ± 0.96
CRA	-0.90 ± 0.51	-1.03 ± 0.53	-0.03 ± 0.10	-0.41 ± 0.48
EP	0.32 ± 0.66	0.83 ± 0.75	-0.47 ± 0.23	-1.28 ± 1.49
VIA	-0.96 ± 0.48	-1.10 ± 0.65	-0.08 ± 0.06	-0.21 ± 0.35

Table 3.2: Absolute difference (mm/day) in precipitation averages at the four representative stations between the observations and the downscaling model simulations for the four prediction methods. The projections are taken from the downscaling results driven by the ensemble of the four climate models.

Projected future winter precipitation obtained using the cross-validation approach for training and bias correction (Figure 3.24) returns values somewhat larger in magnitude than those of the split-record bias correction (for both the ensemble average and common cluster combinations), with ranges of 0% to +11% for average precipitation and +1% to +15% for extreme precipitation. Little variation is seen between the different stations on the island in terms of precipitation anomalies, with the majority of stations experiencing increases of 7% to 9% in average and 9% to 12% in extreme values (the largest projected increases of any of the downscaling methods). Summer precipitation projections based on the cross-validation bias correction approach result in negative anomalies that are localized to a few stations, while the remainder of the sites show little to no difference relative to the baseline. A number of stations concentrated on the southeastern tip of the island are expected to experience decreases in precipitation of −6% to −12%. This pattern is also present in the extreme precipitation, though in that case all stations show negative precipitation anomalies. The decrease observed extremes on the southern stations is as high as −20% with most values in the −10% to −15% range.

Precipitation predictions taken from the statistical model driven by principal components of common EOFs present winter results unlike those seen in the projections made using grid cell averages. Summer precipitation projections resemble those seen in the cross-validation bias correction results. Future summer precipitation is expected to decline most significantly on the eastern and southern shores of Vancouver Island, with anomalies of −10% to −12% at most of those stations. Elsewhere, summer precipitation declines minimally or increases very slightly at stations near Barkley Sound. Winter precipitation projections differ from the other projections both in the spatial distribution of the changes, and in the range of projected changes. The results from this technique display both positive and negative trends, with increases seen on the west coast and decreases observed on the east coast. The magnitudes of the differences are small (mostly less than 10%) and are similar for both average and extreme precipitation when compared to the 20^{th} century baseline.

3.6 Synoptic Typing of Precipitation Occurrence

Making use of the separate statistical model for precipitation occurrence, the projected changes in the frequency of days with measurable precipitation from the end of the 20^{th} century to the end of the 21^{st} century can be determined. To simplify the results, projections

Winter Months						
	Obs. (1971-2000)			Prj. (2081-2100)		
Stations	Mean	95^{th}%	Prct.	Mean	95^{th}%	Prct
CS	8.80	26.00	78.42	7.50	21.00	72.86
CRA	4.50	13.00	63.11	4.00	12.00	59.79
EP	7.50	20.70	74.36	6.40	16.70	70.10
VIA	3.90	10.00	59.25	3.40	8.00	54.71
Summer Months						
	Obs. (1971-2000)			Prj. (2081-2100)		
Stations	Mean	95^{th}%	Prct.	Mean	95^{th}%	Prct
CS	3.50	9.00	55.41	3.30	9.00	54.25
CRA	2.60	7.00	33.01	2.40	6.00	30.68
EP	3.00	8.00	40.52	2.80	7.00	38.59
VIA	2.00	5.00	23.55	1.90	4.00	22.39

Table 3.3: Statistics of extended periods of measurable precipitation at the four representative stations during both winter and summer months. The mean and 95^{th} columns refer to the average and extended lengths of successive days with precipitation. The Prct column lists the percentage of individual days in the dataset with measurable precipitation.

from the four representative stations described previously are presented here as proxies for the different precipitation regimes across the island (Table 3.6). Histograms (Figure 3.26) of the number of consecutive days with non-negligible precipitation from both the baseline and future periods illustrate the changes in the frequency of occurrence of precipitation during both the summer and winter seasons (shown for the split-record bias correction approach here). In all cases, the projected trend for overall precipitation occurrence is one of minor decrease or negligible difference. However, the slight change in the number of days with precipitation masks a more significant change at some stations in the length of intervals of uninterrupted precipitation. During the summer months, the number of days with precipitation at all four of the example stations declines minimally (2.1% to 7.1% decreases) over the twenty-first century. The mean number of successive days with precipitation declines in a similar fashion from -5% to -7.6%, while the drop in extended periods of uninterrupted precipitation is more severe, with decreases of up to 20% (Figure 3.26, changes in the percentiles). This shift is repeated during the winter months. The total number of days with precipitation declines up to 7.7% (Victoria International Airport) and the average lengths of extended stretches of precipitation declines anywhere from 11.1% (Campbell River Airport) to a more significant 20% fewer individual days with measurable precipitation (Victoria International Airport). In short, it rains less often but in bigger amounts.

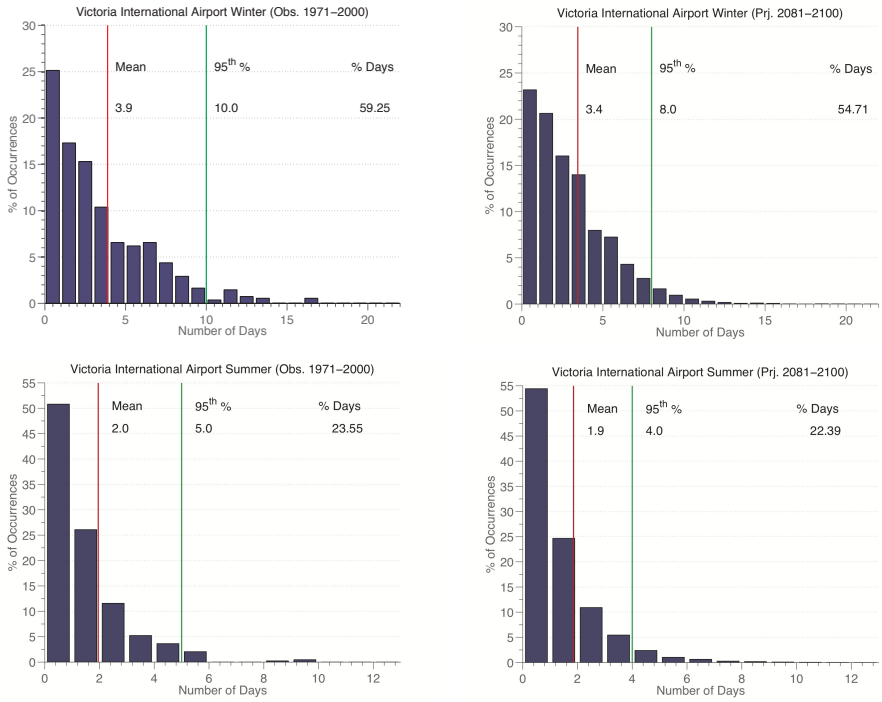

Figure 3.26: Histograms of past and future successive days with nonzero precipitation at Victoria International Airport during the winter and summer seasons. Results are obtained from the split-record, average grid cell approach.

Chapter 4

Discussion

The original test of this statistical downscaling method was over the state of Illinois in the Midwestern United States, a geographically different region than the coastal environment of Vancouver Island. Even though at first glance these two locations have very disparate climates [Kottek et al. (2006)], there are some significant similarities between the two in terms of precipitation occurrence and intensity that enable the present synoptic typing technique in Illinois to be applied successfully to Vancouver Island. Illinois resides in an area with strong seasonal shifts in temperature and precipitation driven by its inland location and prevailing continental air masses [Changnon et al. (2004)]. During the winter months, the presence of the polar jet stream directs low-pressure cells and their accompanying cold fronts over the state, resulting in events with significant precipitation (usually in the form of snowfall). The majority of the region's precipitation is received during the spring and summer, delivered by the passage of convectively driven storms. Though different in cause, Vancouver Island experiences precipitation of the same nature during the winter months, with transient, yet high-intensity precipitation events brought onshore by mid-latitude cyclones. As a result, the same downscaling method applied to Vancouver Island is able to also capture similar features in the precipitation record during different seasons. This study represents the first time this downscaling method has been applied to a coastal area, and the first time that precipitation over Vancouver Island has been studied using statistical downscaling.

In this study the importance of selecting and understanding projected changes in climate model predictor variables is considered to improve the statistical relationships between the large and small scales. Correlation maps evaluated for individual atmospheric variables and island precipitation highlight specific regions and levels of the atmosphere that influence precipitation. The use of multiple grid cells selected based on the strength of their relationship to precipitation over the island (rather than merely choosing the grid cell in closest proximity) ensures that physically relevant, large-scale features influence the statistical model in determining precipitation [Wilby et al. (2004)]. Matching these variables to the synoptic types generated by the hierarchical ascending clustering algorithm reveals distinct atmospheric processes that affect the frequency of occurrence of the different precipitation states.

The synoptic types based on precipitation span a range of intensities and spatial distributions in both the summer and winter seasons. Example synoptic states 1 and 3 in the winter (Figures 3.4, 3.6) and 3 and 5 in the summer (Figures 3.11, 3.13) represent infrequent, high-intensity events with strong west-to-east spatial gradients. These patterns are indicative of events such as mid-latitude cyclones and stand in contrast to the moderate and low intensity states that occur more frequently. The divisions amongst the states suggest the downscaling model is successfully separating the characteristic precipitation into representative types that can effectively simulate the different precipitation regimes that exist on the island. If the synoptic typing had been performed using circulation-based data, the atmospheric patterns may have been more distinct, however the precipitation patterns would have been more alike one another. Choosing between precipitation and atmospheric data to define the synoptic types means recognizing that the data assigned to groups after typing will likely share common features [Vrac et al. (2007)]. From the results of this work, types based on precipitation are capable of capturing the wide range of intensities that occur over Vancouver Island.

The use of precipitation-based synoptic types in conjunction with the Gamma Probability Distribution Function (PDF) goes some way to addressing the deficiencies of using that particular function for the representation of precipitation. One of the major disadvantages of using the Gamma PDF is its ineffectiveness in reproducing the relatively rare, extreme precipitation events that occur under many precipitation regimes [Furrer and Katz (2008)]. Other studies have approached this problem by turning to hybrid distributions, which generally couple the Gamma PDF with another, extreme-value distribution such as the Generalized Paredo [Vrac and Naveau (2007)]. This has shown some improvement in

certain studies, however this issue of fitting distributions with many parameters means these PDFs are less robust, and are less capable at fitting a wide range of precipitation regimes. Additionally, fitting many parameters simultaneously requires more sophisticated optimization routines, which may be unstable when attempting to fit several distributions at many stations. Instead, by dividing the Gamma distribution in part based on intensity, extreme events are relegated to specific synoptic types while low to moderate intensity precipitation are simulated by others. This allows the Gamma PDF better capture the large range of precipitation values by using multiple instances of the PDF, rather than forcing a single distribution to fit such a wide range.

Evidence of the benefit of using a more complex distribution than a single Gamma PDF can be found when attempting to downscale using a single Gamma PDF for each station. In some previous work with downscaling (not detailed here), a Gamma distribution was applied without any synoptic typing. Rather, the two parameters of the PDF were downscaled using multivariate regression. In this case each station precipitation record was fitted with a single Gamma PDF for each season and validation was performed in the same way as in the synoptic typing method. While applying the regression method resulted in seasonal precipitation being effectively fitted with the Gamma distribution, the method was not able to reproduce the seasonal differences present in the observational record. The single Gamma PDF was rarely able to replicate the larger values of precipitation and did not produce a coherent signal among the 34 stations analyzed. This suggested that a single Gamma distribution was insufficient to capture the varied levels of precipitation across the island's weather regimes and led to the use of the synoptic typing based method described earlier.

In figures 3.16 to 3.20 the ability of the statistical downscaling model to recreate past observations is presented. The model is supplied with predictors derived from both NCEP data and climate model data to identify the potential biases that exist due to the potential lack of agreement between climate model data and NCEP Reanalysis data. In general, the forms of downscaling made by climate model predictors were less effective at replicating the historical climatologies than those supplied from NCEP, though not by a large amount. Greater differences were seen between the individual downscaling methods themselves. This demonstrates that while the downscaling method is sensitive to different predictor types, the climate model data is sufficiently accurate to generate the same precipitation statistics as those produced by the NCEP-based predictors.

As mentioned previously, the split record method compares the two, 15 year divisions of the 30 year historical dataset. Training and validation is applied to both halves of the dataset, with one half used to train the other and vice versa. A caveat that must be applied to this form of validation however, is that the statistics of the observed precipitation is not identical in each of the 15 year halves. This is both beneficial and detrimental to the validation process as on the one hand it requires the downscaling method to demonstrate that it is capable of replicating precipitation under a potentially different precipitation regime, however it can also disguise a systemic bias in the downscaling method. This latter effect may explain why the precent differences from the split-record validation results (Figure 3.17) show different magnitudes than those from the cross-validation results (Figure 3.19).

Employing the benefits of synoptic typing and a partitioned Gamma distribution, the downscaling model produced projections for both winter and summer seasons. The magnitude of increases in projected winter precipitation intensity is less than that predicted by the climate models at the large-scale. Precipitation increases projected by the downscaling model (5% to 15% increases depending on the predictor approach) are less that forecast for the end of the century by the climate models' (16% to 20% increase). The downscaling precipitation projections also display little spatial dependence, with stations in all areas of the island experiencing the 5% to 15% increases.

A possible reason for the difference in downscaled and climate model magnitudes is the proximity of Vancouver Island to the Coast Mountain Range and the coarse resolution of the climate models. Examining precipitation maps of the climate model grid cells reveals a high-intensity precipitation band over the southern British Columbian coast that covers both the mainland and the island. With projected increases in winter precipitation expected to be greatest on the windward side of significant topography [Salathe (2008)], there is an expectation for a greater increase in precipitation to occur on the Coast and Cascade Mountain Ranges. The spatial extent of this effect may be extended to cover Vancouver Island as well due to the limited number of grid cells used to recreate both the coastline and the island. The lesser increase projected by the downscaling method omits that influence and likely presents a more accurate picture of the projected increase in precipitation at the end of the 21st century. This result is further strengthened by the similar magnitudes of winter precipitation increases found by past studies along the coastal areas compared to the mountain ranges [Salathe et al. (2007); Salathe (2005); Leung et al. (2004)].

Within the results for projected winter precipitation intensity, a lack of a distinct spatial trend exists across the area of Vancouver Island. A possible interpretation of this pattern is that because all of the stations are located on or near the coast with few exceptions, the projected values are showing the same trend as the regional climate models (RCM). That is, they show gradients of increasing precipitation intensity from the coastline to high altitudes rather than from one side of the island to the other. This could mean that the results are accurate, and that due to the lack of elevated stations there are not any records to represent the larger increases expected in those regions. An evaluation of this method on an area with both low elevation, coastal stations and high altitude stations possessing long-term precipitation records would serve to confirm whether this theory is correct.

The downscaling model predicts more varied results during the summer months, with greater disparity in the size of the projected anomalies from station to station. Both common EOF and cross-validation results for summer precipitation capture a distinct spatial trend, with the greatest reduction in intensity observed on the southern and eastern regions of the island. The pattern likely arises from a decrease in precipitation on the leeward side of mountain ranges in the Pacific Northwest. As the prevailing winds during the summer months are projected to intensify slightly by the end of the 21st century [Merryfield et al. (2009)], northwesterly winds encountering the Beaufort Mountain Range along the length of the island will likely strengthen during the summer months. In the split-record and common cluster approaches, other spatial dependences are evident in the magnitudes, with the statistically significant declines occurring at individual stations (split-record, Figure 3.22), or on the west coast and southern tip of the island (common cluster, Figure 3.23). The drier west coast stations of the common cluster projections could still be due to the same strengthening of the northwesterly winds, causing drier air to subside over the sides of the Beaufort Mountain Range. At other individual stations elsewhere on the island, larger decreases seen in both the common cluster and split-record method may be due to the different form of bias correction applied using the different methods and thus the range of projections offered must be considered. The true spatial dependence of the precipitation anomalies is an especially important mechanism to quantify accurately, as the majority of watersheds for community water resources on Vancouver Island lie on the leeward side of the mountain ranges along the spine of the island and would be affected by such a process [B.C. Ministry of Environment (2007)].

The effect of differences between the predictor forms (averaged grid cells, common EOFs) and combinations (ensemble, common clustering) on the simulated precipitation are evident

in both the validation and projection results. In the case of averaged large-scale grid cells and common EOFs, the two predictor types cover different spatial regions, with the average predictors spanning those grid cells selected by the correlation maps while the EOFs are decomposed from grid cells spanning the entire Northeast Pacific. The larger area of the Northeast Pacific includes more of the storm tracks, more of the semi-permanent pressure cells, and more of the regions projected to experience greater change than those nearer to the coast. These other influences may explain why the projections made by the common EOF experiment show traits (such as both positive and negative precipitation anomalies in winter) and different validation results that are not seen in the other experiments. Nevertheless, the fact that the validation results between the NCEP-based and climate model-based, common EOF results display very different patterns (a result not seen in the validations using averaged grid cells) means the projections from this particular method must be used carefully.

The differences between the ensemble and common cluster approaches suggest the method by which information from different climate models are combined may need to be considered more thoroughly. As the only difference between these two methods was the point when the climate models were combined (before or after the application of the same downscaling model), the different results would likely be independent of whatever downscaling technique is applied. The method of forming a model ensemble, when it should be done, whether a weighting scheme can or should be applied to the input of the selected climate models must be taken into account, especially when comparing one study to another. As the validation results from the different methods based on averaged climate model grid cells are not dramatically different, any one if the individual results cannot be taken as superior to all the others. Instead, the results are better analyzed as an ensemble much like the large-scale climate models are considered. The results from the various downscaling methods provide brackets for the precision of the projections at each station when subject to similar but not identical predictors. This technique gives estimates of overall precipitation changes that are based on multiple inputs, and therefore less subject to the potential issues of a single method.

The separate Markov model designed to handle precipitation occurrence performed effectively, with all stations showing negligible differences or minor underestimation in the validation experiments. Correcting for these discrepancies and focusing on the four example stations reveals projected precipitation occurrence is not expected to deviate dramatically from the present conditions (Figure 3.26). Notably, the sign of the changes are the same

in both seasons in contrast to the different projections of precipitation intensity. This suggests the overall trend is a shift towards less frequent, but more intense precipitation events during the winter months. An increase in such events would potentially result in greater weather-induced damage to vulnerable infrastructure such as flooding. Simultaneous declines in both precipitation intensity and occurrence during the summer months will likely lead to greater stress on water supplies in communities in the affected areas. At present, periods without measurable precipitation can extend for weeks at a time on the south and east coasts of the island during the summer months. As the frequency of these situations increase, the capacity of reservoirs and groundwater aquifers will need to be evaluated to determine if the present infrastructure is sufficient to handle them [B.C. Ministry of Environment (2007); Lemmen et al. (2007)].

Fewer studies are available for comparison of simulated days with precipitation, as a significant number only focus on the seasonal or annual totals and do not conduct experiments at the daily scale necessary to resolve the individual precipitation events. However, in examinations of precipitation occurrence over the Pacific Northwest, an increased likelihood of extreme events is projected [Christensen et al. (2007); Held and Snoden (2006)]. In the study over Illinois [Vrac et al. (2007)], the use of precipitation to define synoptic types resulted in better agreement between the distribution of wet-day lengths than those produced by the types generated from large-scale circulation variables. Further, investigation of the separation between precipitation amount and occurrence had previously noted the success of Markov models in representing occurrence [Gregory et al. (1993)]. This success was also found in this study, with precipitation occurrence captured at the weather stations with only a small underestimation that was common to all stations (Figure 3.26). The different trends seen between the projections for precipitation intensity and occurrence reinforce the need to examine both of these components of precipitation in order to fully understand how precipitation regimes may be altered under projected climate change.

Common to all of the future precipitation projections is that the magnitudes from each of the different methods are the same size or smaller than their respective biases seen in the validation experiments. The larger biases suggest the results from the downscaling experiments must be interpreted with some degree of caution. Bias correction adjusts the projections to account for the separation between the model simulations and observations, however that correction assumes a systemic bias on the part of the downscaling model that remains the same regardless of the time examined. The use of multiple variations of the downscaling method, coupled with repeated simulations of the same downscaling

configuration help to increase confidence in the range of results provided. As well, that the results match the general trends of the large-scale projections [Christensen et al. (2007)], and those of other statistical downscaling experiments in nearby locations [Salathe et al. (2007); Salathe (2005); Leung et al. (2004)] is also encouraging. Nevertheless, the magnitude of the biases, and the fact that this is the first study of its type for this particular region suggest the results should be used carefully.

Repeated experiments with the statistical model driven by the same predictor variables over the same time period eliminates some of the variability in the projected precipitation associated with the stochastic nature of the model. These repeated experiments also provide estimates of the model uncertainty associated with each projection or simulation at each station as a distribution of projected values is produced in each case. The spread in the simulated values at each station then determines whether the difference between the simulations and the observations is significant at the 5% significance level. In the validation experiments, nearly all results demonstrate a statistically significant difference from the validation observations, confirming the presence of a bias in the statistical method that must be corrected. These measures take into account neither the implicit uncertainty associated with the climate models themselves [Dibike et al. (2008)], nor the uncertainty in the $SRESA2$ emissions scenario [Nakicenovic and coauthors (2000)]. Additionally, clustering the observations into synoptic types reduces the precipitation information (as the entire dataset must be described by a finite number of types), resulting in some loss of variability. Assuming randomly distributed errors in the climate models means using an ensemble should eliminate uncertainty in the models to some degree, however the actual uncertainty of the climate model projections and how these evolve over the 21st century are not explicitly included in the analysis.

Additionally, this downscaling method is limited to developing statistical relationships between large-scale model output and station scale weather information only from the latter thirty years of the 20^{th} century. The finite time interval potentially restricts the SD techniques from capturing longer-term variability that may exist in both model and observational records. While the observational record identifies the interannual and decadal variability in seasonal precipitation, it is unable to discern multi-decadal variability from any simultaneous secular trend [Ault and George (2010)]. Precipitation variability at these lower frequencies cannot be readily distinguished from the observed trend of increasing winter precipitation in the weather station data. However, Ault et al. (2010) found that decadal to multi-decadal variability was not a significant component of the precipitation

record, rather that it is interannual variability combined with an increasing secular trend [Zhang et al. (2000)] that contributes to the observed seasonal changes.

While the weather stations employed in this study were situated in various precipitation regimes, they were largely confined to the coastline of the island and none were located at high altitude (the highest station was situated at 231 m above sea level). As a result, the precipitation observations are biased towards sea level and coastal environments, and are less useful for the investigation of precipitation dependent features such as snowpack, or river catchment basins. Their positions also limit the ability of methods such as geographical interpolation [Benestad et al. (2008); Steig et al. (2008)] to extend the point source station results of the downscaling technique to regions at higher elevations that may not have long-term records of precipitation. Analysis of climate model output for Vancouver Island [Christensen et al. (2007); Salathe (2006)] suggests increases in winter precipitation are most significant on the windward sides of elevated topographic features. Downscaling results in these regions would verify that these models are correctly capturing the projected trend over the 21^{st} century. Unfortunately, due to the scarcity of any long-term precipitation records in these areas, statistical downscaling of any kind will be of limited use for analyzing precipitation trends in the alpine regions of Vancouver Island.

Recently, as computing resources have expanded, Regional Climate Models (RCM) have become more commonly used to improve the resolution of future climate projections. Also known as "dynamical downscaling", RCMs provided projections at resolution on the order of kilometres, and are not restricted to areas with weather station records as is the case for statistical downscaling. These smaller scale models are usually "nested" in, or forced by boundary conditions from large scale climate models and are used over specific regions such as that of the province of British Columbia. Results of previous RCM studies for the Pacific Northwest and coast British Columbia have identified contradictory trends in seasonal precipitation over the 21^{st} century. Salathe [Salathe (2008)] conducted simulations of the coastal climate with the ECHAM5-MM5 RCM producing projections of precipitation for the standard meteorological seasons of DJF, MAM, JJA, SON. The RCM output predicted decreased precipitation intensity during the fall/winter seasons (SON, DJF) and small increases in precipitation intensity during the spring/summer seasons. In contrast, projections for the same area using the Canadian Regional Climate Model (CRCM4) forced by the Canadian Global Climate Model (CGCM3) using the same emissions scenario produced very different projections [B.C. Ministry of Environment (2007)], with more typical winter increases and summer decreases in precipitation intensity.

The significant computer resources that the RCMs require renders multi-model ensemble of RCMs impractical. It also means a typical RCM can only be employed with a single large scale model to provide boundary conditions, as to use more would be too computationally expensive. Statistical downscaling can provide such multi-model projections efficiently and can be used to evaluate multiple climate scenarios in order to generate ensemble projections. As such, there will always be the need for independent methods such as statistical downscaling to corroborate the projections made by the continually evolving large scale and regional climate models.

Chapter 5

Conclusions

Synoptic typing based on precipitation observations produced distinct representative states of both precipitation and circulation, which were used to represent the historical precipitation records. Each of the precipitation states' distributions of precipitation was matched with the physical influences of the varying, prevailing, westerly winds and the local topography that affect the distribution of precipitation on Vancouver Island. Similarly, composites of atmospheric circulation associated with each precipitation type captured the dynamical processes that influence precipitation. Winter northward shifts in the North Pacific storm tracks and northward movement ofs the Aleutian Low were reflected in the increased winter precipitation produced by the downscaling model. Enhancement of the existing summer, northwesterly wind patterns resulted in a drying trend during the summer season, over the region of the island in the lee of the Beaufort Mountain Range.

Examining each of the downscaling experiments validation results revealed a systemic underestimation of observed precipitation that was common to all of the methods, except for the experiment employing principal components of climate model, common EOFs as predictor variables, which displayed both wet and dry biases. Winter precipitation intensity was best replicated by the common EOF approach in average and by the split-record approach for extreme precipitation. Summer average precipitation intensity was best captured by the split-record method and extreme precipitation was reproduced most successfully by the common EOF approach (though likely due to the wet bias of the method). Using the model

projections from the SRES A2 scenario, the statistical model predicted moderate increases in average (5% to +10%) and up to +20% in extreme precipitation intensity during the winter months over the entirety of Vancouver Island. Summer months experience reductions (6% to 20%) in both average and extreme precipitation. While winter precipitation increases are spread uniformly across the area of the island, summer precipitation reduction exhibit a strong spatial dependence, declining most significantly over the southern half of the island. Precipitation occurrence declines modestly in both seasons, with reductions of 2% to 7% in the total number of days with precipitation and up to a 20% in the length of extended periods of continuous precipitation. The differences in magnitude and spatial distribution in the downscaling projections compared to the large-scale climate model results highlight the role of small-scale processes in defining precipitation, and demonstrate the need for high-resolution methods to convert climate model output to relevant, regional scales.

Bibliography

Alexander, M., Blade, I., Newman, M., Lanzante, J., Ngar-Cheung, L., and Scott, J. (2002). The atmospheric bridge: The influence of enso teleconnections on air-sea interaction over the global oceans. *Journal of Climate*, 15:2205–2231.

Apipattanavis, S., Podesta, G., Rajagopalan, B., and Katz, R. (2007). A semiparametric multivariate and multisite weather generator. *Water Resources Research*, 43:19.

Ault, T. and George, S. S. (2010). The magnitude of decadal and multidecadal variability in north american precipitation. *Journal of Climate*, 23:842–850.

B.C. Ministry of Environment (2007). Environmental trends in british columbia: 2007. Technical report, State of Environment Reporting.

Bellone, J., Hughes, J., and Guttorp, P. (2000). A hidden markov model for downscaling synoptic atmospheric patterns to precipitation amounts. *Climate Research*, 15:1–12.

Benestad, R. (2001). A comparison between two empirical downscaling strategies. *International Journal of Climatology*, 21:1645–1668.

Benestad, R., Hanssen-Bauer, I., and Chen, D. (2008). *Empirical Statistical Downscaling*. World Scientific Publishing Co. Pte. Ltd.

Bjornsson, H. and Venegas, S. (1997). *A manual for EOF and SVD analyses of climatic data*. Department of Atmospheric and Ocean Sciences and Centre for Climate and Global Change Research, McGill University, Montreal, Canada.

Bridges, T. and Haan, C. (1972). Reliability of precipitation probabilities estimated from the gamma distribution. *Monthly Weather Review*, 100:607–611.

Changnon, S., Angel, J., Kunkel, K., and Lehmann, C. (2004). *Illinois Climate Atlas*. Illinois State Water Survey.

Charles, S., Bates, B., Smith, I., and Hughes, J. (2004). Statistical downscaling of daily precipitation from observed and modelled atmospheric fields. *Hydrological Processes*, 18:1373–1394.

Cheng, C., Auld, H., Li, G., Klaassen, J., and Li, Q. (2007). Possible impacts of climate change on freezing rain in south-central canada using dowscaled future climate scenarios. *Natural Hazards and Earth System Sciences*, 7:71–87.

Christensen, J., Hewitson, B., Busuioc, A., Chen, A., Gao, X., Held, I., Jones, R., Kolli, R., Kwon, W.-T., Laprise, R., Rueda, V. M., Mearns, L., Menéndez, C., Räisänen, J., Rinke, A., Sarr, A., and Whetton, P. (2007). *Regional Climate Projections. In: Climate Change 2007: The Physical Science Basis. Contribution of Working Group I to the Fourth Assessment Report of the Intergovernmental Panel on Climate Change.* Cambridge University Press, Cambridge, United Kingdom and New York, NY, USA.

Cuell, C. and Bonsal, B. (2009). An assessment of climatological synoptic typing by principal component analysis and kmeans clustering. *Theoretical and Applied Climatology*, 98:361–373.

Dibike, Y., Gachon, P., St-Hilaire, A., Ouarda, T., and Nguyen, V. T.-V. (2008). Uncertainty analysis of statistically downscaled temperature and precipitation regimes in northern canada. *Theoretical and Applied Climatology*, 91:149–170.

Elsner, M. M., Littell, J., and Binder, L. W. (2009). *The Washington Climate Change Impacts Assessment: Evaluating Washington's Future in a Changing Climate.* Center for Science in the Earth System, Joint Institute for the Study of the Atmosphere and Oceans, University of Washington, Seattle, Washington.

Environment Canada (2010). Climate data online.

Fowler, H., Blenkinsop, S., and Tebaldi, C. (2007). Review: Linking climate change modelling to impacts studies: recent advances in downscaling techniques for hydrological modelling. *International Journal of Climatology*, 27:1547–1578.

Furrer, E. M. and Katz, R. (2008). Improving the simulation of extreme precipitation events by stochastic weather generators. *Water Resources Research*, 44:13.

Gregory, J., Wigley, T., and Jones, P. (1993). Application of markov models to area-average daily precipitation series and interannual variability in seasonal totals. *Climate Dynamics*, 8:299–310.

Hannachi, A., Jolliffe, I., and Stephenson, D. (2007). Empirical orthogonal functions and related techniques in atmospheric science: A review. *International Journal of Climatology*, 27:1119–1152.

Held, I. and Snoden, B. (2006). Robust responses of the hydrological cycle to global warming. *Journal of Climate*, 19:5686–5699.

Hellstrom, C., Chen, D., Achberger, C., and Raisanen, J. (2001). Comparison of climate change scenarios for sweden based on statistical and dynamical downscaling of monthly precipitation. *Climate Research*, 19(45-55).

Hewitson, B. and Crane, R. (1996). Climate downscaling: techniques and application. *Climate Research*, 7:85–95.

Hughes, J., Guttorp, P., and Charles, S. (1999). A nonhomogeneous hidden markov model for precipitation. *Applied Statistics*, 48:15–30.

Kalnay, E. and coauthurs (1996). The ncep/ncar 40-year reanalysis project. *Bulletin of the American Meteorological Society*, 77:437–470.

Konrad, C. (1997). Synoptic-scale features associated with warm season heavy rainfall over the interior southeastern united states. *Weather and Forecasting*, 12:557–571.

Kottek, M., Grieser, J., Beck, C., Rudolf, B., and Rubel, F. (2006). World map of the koppen-geiger climate classification updated. *Meteorologische Zeitschrift*, 15(259-263).

Lemmen, D., Warren, F., Lacroix, J., and Bush, E. (2007). *From Impacts to Adaptation: Canada in a Changing Climate 2007*. Government of Canada.

Leung, L., Qian, Y., Bian, X., Washington, W., Han, J., and Roads, J. (2004). Mid-century ensemble regional climate change scenarios for the western united states. *Climatic Change*, 62:75–113.

Mass, C. (2008). *The weather of the Pacific Northwest*. University of Washington Press.

Meehl, G., Covey, C., Delworth, T., Latif, M., McAvaney, B., Mitchell, J. F. B., Stouffer, R. J., and Taylor, K. E. (2007). The wcrp cmip3 multi-model dataset: A new era in climate change research. *Bulletin of the American Meteorological Society*, 88:1383–1394.

Merryfield, W., Pal, B., and Foreman, M. (2009). Projected future changes in surface marine winds off the west coast of canada. *Journal of Geophysical Research*, 114.

Milnes, E., Elsner, M., Litell, J., Binder, L. W., and Lettenmaier, D. (2010). Assessing regional impacts and adaptation strategies for climate change: the washington climate change impacts assessment. *Climatic Change*, 99:19.

Myoung, B. and Deng, Y. (2009). Interannual variability of the cyclonic activity along the u.s. pacific coast: Influences on the characteristics of winter precipitation in the western united states. *Journal of Climate*, 22:5732–5747.

Nakicenovic, N. and coauthors (2000). *Special Report on Emissions Scenarios: A Special Report of Working Group III of the Intergovernmental Panel on Climate Change*. Cambridge University Press.

Paul, S., Liu, C., Chen, J., and Lin, S. (2008). Development of a statistical downscaling model for projecting monthly rainfall over east asia from a general circulation model output. *Journal of Geophysical Research*, 113.

Salathe, E. (2003). Comparison of various precipitation downscaling methods for the simulation of streamflow in a rainshadow river basin. *International Journal of Climatology*, 23:887–901.

Salathe, E. (2005). Downscaling simulations of future global climate with application to hydrologic modelling. *International Journal of Climatology*, 25:419–436.

Salathe, E. (2006). Influences of a shift in north pacific storm tracks on western north american precipitation under global warming. *Geophysical Research Letters*, 33.

Salathe, E. (2008). A high-resolution climate model for the u.s. pacific northwest: Mesoscale feedbacks and local responses to climate change. *Journal of Climate*, 21:5708–5726.

Salathe, E., Mote, P., and Wiley, M. (2007). Review of scenario selection and downscaling methods for the assessment of climate change impacts on hydrology in the united states pacific northwest. *International Journal of Climatology*, 27:1611–1621.

Schuenemann, K. and Cassano, J. J. (2010). Changes in synoptic weather patterns and greenland precipitation in the 20th and 21st centuries 2: Analysis of 21st century atmospheric changes using self-organizing maps. *Journal of Geophysical Research: Atmospheres*, 115:18.

Stahl, K., Moore, R., and McKendry, I. (2006). The role of synoptic-scale circulation in the linkage between large-scale ocean-atmosphere indices and winter surface climate in british columbia, canada. *International Journal of Climatology*, 26(541-560).

Steig, E., Schneider, D., Rutherford, S., Mann, M., Comiso, J., and Shindell, D. (2008). Warming of the antarctic ice-sheet surface since the 1957 international geophysical year. *Nature*, 457:459–462.

Tim, O. and Diaz, H. (2009). Synoptic-statistical approach to regional downscaling of ipcc twenty-first-century climate projections: Seasonal rainfall over the hawaiian islands. *Journal of Climate*, 22:4261–4280.

Trenberth, K. and Hurrell, J. (1994). Decadal atmosphere-ocean variations in the pacific. *Climate Dynamics*, 9(303-319).

Vrac, M. and Naveau, P. (2007). Stochastic downscaling of precipitation: from dry events to heavy rainfalls. *Water Resources Research*, 43:13.

Vrac, M., Stein, M., and Hayhoe, K. (2007). Statistical downscaling of precipitation through nonhomogeneous stochastic weather typing. *Climate Research*, 34:169–184.

Widmann, M., Bretherton, C., and Jr., E. S. (2003). Statistical precipitation downscaling over the northwestern united states using numerically simulated precipitation as a predictor. *Journal of Climate*, 16:799–816.

Wilby, R., Charles, S., Zorita, E., Timbal, B., Whetton, P., and Mearns, L. (2004). Guidelines for use of climate scenarios developed from statistical downscaling methods. Supporting material of the Intergovernmental Panel on Climate Change.

Wilks, D. (1995). *Statistical methods in the atmospheric sciences*. Academic Press.

Yarnal, B., Comrie, A., Frakes, B., and Brown, D. (2001). Developments and prospects in synoptic climatology. *International Journal of Climatology*, 21:1923–1950.

Zhang, X., Vincent, A., Hogg, W., and Niitsoo, A. (2000). Temperature and precipitation trend in canada during the 20th century. *Atmosphere-Ocean*, 38:395–429.